

## **General Disclaimer**

### **One or more of the Following Statements may affect this Document**

- This document has been reproduced from the best copy furnished by the organizational source. It is being released in the interest of making available as much information as possible.
- This document may contain data, which exceeds the sheet parameters. It was furnished in this condition by the organizational source and is the best copy available.
- This document may contain tone-on-tone or color graphs, charts and/or pictures, which have been reproduced in black and white.
- This document is paginated as submitted by the original source.
- Portions of this document are not fully legible due to the historical nature of some of the material. However, it is the best reproduction available from the original submission.

NASA CR-167873

(NASA-CR-167873) ATMOSPHERIC RADIATION  
MODEL FOR WATER SURFACES Final Technical  
Report, 4 Mar. 1981 - 15 Jul. 1982 (Science  
Applications, Inc.) 67 p HC A04/MF A01

N 83-21677

Unclassified  
03211



# SCIENCE APPLICATIONS, INC.

NASA CR-167873  
SAI-82-002-AA

ATMOSPHERIC RADIATION  
MODEL FOR  
WATER SURFACES

FINAL TECHNICAL REPORT

ROBERT E. TURNER  
DANIEL W. GASKILL  
JAMES R. LIERZER

SCIENCE APPLICATIONS, INC.  
1010 WOODMAN DRIVE, SUITE 200  
DAYTON, OHIO 45432

MAY 1982

PREPARED FOR  
NATIONAL AERONAUTICS AND SPACE ADMINISTRATION  
LEWIS RESEARCH CENTER  
CLEVELAND, OHIO 44135  
CONTRACT NO. NAS3-22495

UNCLASSIFIED

**SECURITY CLASSIFICATION OF THIS PAGE (When Data Entered)**

UNCLASSIFIED

SECURITY CLASSIFICATION OF THIS PAGE(When Data Entered)

additional components such as the atmospheric path radiance which results from singly-scattered sky radiation specularly reflected by the water surface. It also considers a component which is referred to as the virtual sun path radiance, i.e. the singly-scattered path radiance which results from the solar radiation which is specularly reflected by the water surface.

These atmospheric radiation components are coded into a computer program for the analysis of multispectral remote sensor data over the Great Lakes of the United States. The user must know certain parameters, such as the visibility or spectral optical thickness of the atmosphere and the geometry of the sensor with respect to the sun and the target elements under investigation.

Suggestions and recommendations are given for further investigation of the problem of the remote sensing of water surfaces. If all of these extrinsic radiation components are properly accounted for, then the intrinsic water radiance can be found by applying the algorithm or an adaptation of the algorithm in this report. As a result, one would then be able to know the actual surface water spectral radiation field independent of the atmosphere.

ORIGINAL PAGE IS  
OF POOR QUALITY

UNCLASSIFIED

## PREFACE

This report describes part of the work done on a research program in the remote sensing of the Great Lakes using a multi-spectral scanner aboard an aircraft. The research has been conducted for the NASA-Lewis Research Center, Cleveland, Ohio, by Science Applications, Inc., at the Dayton, Ohio, office. The primary objective of this program is to develop remote sensing as a practical technique for the analysis of the Great Lakes.

Remote sensing of the environment involves the transfer of radiation from the Earth's surface through the atmosphere to a sensor which is located at some point within the atmosphere. For water surfaces with their inherently low reflectances, the atmospheric scattering of solar radiation acts as a significant noise factor. In this report we have extended an existing model to include various atmospheric radiation components so that the resulting mathematical algorithm will allow one to extract a radiance value which is more nearly representative of the actual radiance of the water, independent of atmospheric effects.

This research was performed under contract NAS3-22495 and covers the period from 4 March 1981 through 15 July 1982. Mr. Thom Coney served as Technical Monitor of the contract and Dr. Robert E. Turner of Science Applications, Inc., was the program manager and principal investigator.

## CONTENTS

	<u>Page</u>
PREFACE . . . . .	iii
TABLE OF CONTENTS . . . . .	iv
FIGURES . . . . .	v
TABLES . . . . .	vii
1. SUMMARY . . . . .	1
2. INTRODUCTION . . . . .	2
3. OPTICAL PROPERTIES OF WATER . . . . .	4
3.1 REFLECTION, REFLECTANCE AND REFRACTION . . . . .	4
3.2 ABSORPTION AND SCATTERING . . . . .	10
3.3 OPTICAL PROPERTIES OF A WIND RUGHENED WATER SURFACE . . . . .	11
4. COMPONENTS OF REFLECTED AND PATH RADIANCE IN REMOTE SENSING OVER WATER . . . . .	14
4.1 REFLECTED SKY RADIANCE, $L_{SKYR}$ . . . . .	14
4.2 SINGLY SCATTERED REFLECTED SOLAR RADIANCE, $L_{VP}$ . . . . .	19
4.3 SINGLY SCATTERED PATH RADIANCE, $L_{PSS}$ . . . . .	22
4.4 MULTIPLY SCATTERED PATH RADIANCE, $L_{PMS}$ . . . . .	24
5. COMPUTER MODEL AND RESULTS . . . . .	25
5.1 SPECIFICATION OF SOLAR AND SENSOR GEOMETRY . . . . .	25
5.2 ATMOSPHERIC CORRECTION OPTIONS . . . . .	26
5.3 MODEL INPUT PARAMETERS . . . . .	27
5.4 MODEL CALCULATIONS . . . . .	42
6. CONCLUSIONS AND RECOMMENDATIONS . . . . .	53
REFERENCES . . . . .	55

## FIGURES

	<u>Page</u>
1. Specular Reflection From a Smooth Water Surface . . . . .	5
2. Refraction of the Transmitted Beam at the Water Surface and the Law of Refraction . . . . .	6
3. Fresnel Reflectance for Unpolarized Light as a Function of Angle of Incidence of Incoming Beam . . . . .	8
4. Fresnel Reflectance and Transmittance as a Function of Angle of Incidence of Incoming Beam . . . . .	9
5. Components of Total Radiance Detected by Sensor . . . . .	15
6. Geometry for Reflected Sky Radiance Computation . . . . .	16
7. Geometry for Virtual Sun Path Radiance Calculation . . . .	20
8. Geometry for Singly Scattered Path Radiance . . . . .	23
9. Scan Plane and Solar Geometry . . . . .	26
10. Singly-Scattered Reflected Sky Radiance at Sensor for a Wavelength of 0.55 $\mu\text{m}$ . . . . .	43
11. Singly-Scattered Virtual Path Radiance at Sensor for a Wavelength of 0.55 $\mu\text{m}$ . . . . .	44
12. Surface and Path Radiance Components Detected by Sensor at Optical Depth of $\tau = 0.346$ as a Function of Scan Angle . . . . .	45
13. Ratio of Reflected Singly Scattered Sky Radiance to Singly Scattered Path Radiance as a Function of Scan Angle . . . . .	47
14. Ratio of Singly Scattered Path Radiance from the Virtual Sun, $L_{\text{VP}}$ , to Singly Scattered Path Radiance, $L_{\text{PSS}}$ , as a Function of Scan Angle . . . . .	48
15. Ratio of Multiply Scattered Path Radiance, $L_{\text{PMS}}$ , to Singly Scattered Path Radiance, $L_{\text{PSS}}$ , as a Function of Scan Angle . . . . .	49
16. Ratio of Reflected Sky Radiance to Singly Scattered Path Radiance for Three Continental Aerosol Models . . . . .	50

FIGURES (Cont'd)

	<u>Page</u>
17. Ratio of Singly Scattered Path Radiance from the Virtual Sun, $L_{VP}$ , to Singly Scattered Path Radiance, $L_{PSS}$ , as a Function of Atmospheric Visibility for Three Continental Aerosol Models . . . . .	51
18. Ratios of (a) $L_{VP}/L_{PSS}$ , (b) $L_{SKYRE}/L_{PSS}$ , (c) $L_{SKYRE}/L_{VP}$ as a Function of Visibility (KM) . . . . .	52

**TABLES**

	<u>Page</u>
1. Input File on Logical Unit 4 for Use by ATMSFR . . . . .	28
2. Program Listing .	30

## SYMBOLS

$E_0$	solar irradiance at the top of the atmosphere
$E_0'$	solar irradiance of the virtual sun
$L_0(i)$	radiance incident at angle $i$
$L_s(i)$	surface radiance at angle $i$
$L_{SKYRE}$	reflected sky radiance
$L_{SOLRE}$	reflected solar radiance
$L_{SKY}$	sky radiance
$L_{SOL}$	direct beam radiance
$L_{PMS}$	multiply scattered path radiance
$L_{PSS}$	singly scattered path radiance
$L_U$	upward scattered radiance beneath water surface
$L_{INIR}$	radiance scattered from beneath water surface
$L_{SKYSS}$	singly scattered sky radiance
$L_{PTOT}$	total radiance
$L_{VSOL}$	radiance from virtual sun
$L_{VP}$	virtual sun path radiance
$n$	index of refraction of water relative to air
$p$	slope probability
$p(x)$	scattering phase function
$T$	transmittance

### (GREEK SYMBOLS)

$\theta_i$	incident angle
$\theta_r$	reflected angle
$\rho_s$	Fresnel reflectance

$\rho_f(i)$	Fresnel reflectance at angle i
$\theta$	nadir view angle
$\theta_0$	solar zenith angle
$\phi$	azimuth view angle
$\phi_0$	solar azimuth angle
$\mu$	cosine of nadir view angle
$\mu_0$	cosine of solar zenith angle
$\chi_{SKY}$	scattering angle
$\tau$	optical depth
$\tau_0$	optical thickness
$\eta$	forward scattering parameter
$\rho$	surface albedo
$\omega_0$	single scattering albedo

## SUMMARY

In the analysis of remotely sensed data on bodies of water, the atmosphere obscures the inherent surface features as a result of the scattering and absorption of solar radiation. In the case of multispectral data acquired by aircraft or spacecraft sensors, one can preprocess the data by applying mathematical models and algorithms to the digitized data. The mathematical model developed in this investigation is specifically designed to account for various components of the visible and infrared radiation in the atmosphere which interfere with the inherent signal from a water surface. If the atmospheric parameters are known, then when the algorithm is applied to the multispectral data sets, an improved or corrected data set will result.

This improved atmospheric correction model allows for the path radiance in the atmosphere as a result of singly-scattered solar radiation and also singly-scattered solar-reflected radiation. In addition, the model includes a singly-scattered sky radiation component for the radiation which is reflected by the water surface. Comparisons are made among the relative magnitudes of these radiation components in terms of the geometric and environmental factors. Recommendations are presented for a more advanced model which would include the corresponding radiation components for multiple scattering.

## INTRODUCTION

Multispectral scanner data obtained by sensors aboard aircraft and spacecraft allow a user to examine the detailed physical properties of a surface. These properties are of interest to many investigations in various disciplines such as land use studies, agriculture, hydrology, forestry, and oceanography. In all of these investigations, however, the scattering of visible and infrared radiation by the atmospheric constituents will reduce the inherent surface radiance and add a path radiance to the attenuated radiance from the target. For many cases of the remote sensing of bright land areas on relatively clear days the attenuated radiation from the surface is rather large as compared to the atmospheric path radiance. For water bodies, with inherently low reflectances, this is no longer true and the path radiance can be a major effect in the total radiance at the sensor.

The purpose of this investigation was to extend an existing atmospheric radiative transfer model to include other radiation components which did not exist in the previous model. These additional atmospheric radiation components include specific effects for the remote sensing of water surfaces. The model is used in conjunction with an algorithm specifically designed for the analysis of multispectral data.

The determination of the atmospheric radiation components is important for the analysis of the probability of misclassification of various classes of surface materials. To first order one may consider the so called linear transfer problem in which the path radiance is constant over varying surface reflectances for a horizontally spatially uniform haze. For a non-uniform haze, however, the path radiance can vary, thereby resulting in a higher

probability of misclassification of objects if the degree of non-uniformity is unknown. A second-order effect, but one which can become quite important for the remote sensing of high-contrast targets is the adjacency effect. This is when radiation from a bright target causes an increase in the path radiance with respect to the radiance from a neighboring dark target. This problem would exist, for example, in the remote sensing of water bodies near bright sandy beaches. The results should be evident in the brightened image of the water near the shoreline, provided the effects of waves and whitecaps are eliminated. This second-order adjacency effect is not included in the model or algorithm in this investigation but the effect can be accounted for if the investigator has sufficiently detailed atmospheric data on the horizontal stratification of aerosols.

Multiple scattering is particularly important if the sky is hazy. These effects are considered in the model for path radiance which results from the sun as a source. We have not included the multiple scattering effects for solar-reflected radiation.

## OPTICAL PROPERTIES OF WATER

The interpretation of remote sensing data collected over water surfaces requires a detailed knowledge of the optical properties of water and the air-water interface. Water is unusual as a natural surface because it is a specular reflector and because in the visible regions sensible data can be obtained from well below the water surface [1]. Also of importance is the phenomenon of refraction, which occurs when radiation passes through the air-water boundary. These properties of water and their significance in terms of remote sensing are discussed in detail in this chapter.

### 3.1 REFLECTION, REFLECTANCE AND REFRACTION

Most natural surfaces are approximately Lambertian--reflecting incident radiance equally in all directions. A smooth water surface, however, is a specular reflector, and reflection of radiation from it follows the geometrical law of reflection. This geometric law requires that the angle with respect to the normal to the surface of the reflected ray equal the angle of incidence of the incident ray and that the reflected ray be in the same plane as the incident ray. Specular reflection is depicted in Figure 1. Reflectance,  $\rho_s$ , of the water surface is given by the Fresnel equation

$$\rho_s = \frac{1}{2} \left[ \frac{\sin^2(\theta_i - \theta_r)}{\sin^2(\theta_i + \theta_r)} + \frac{\tan^2(\theta_i - \theta_r)}{\tan^2(\theta_i + \theta_r)} \right], \quad (1)$$

where  $\theta_i$  is the incident angle and  $\theta_r$  is the angle of refraction.

The transmitted part of the incident ray experiences refraction at the water surface, as shown in Figure 2. Snell's law, given by

$$\frac{\sin(\theta_i)}{\sin(\theta_r)} = n, \quad (2)$$

ORIGINAL PAGE IS  
OF POOR QUALITY

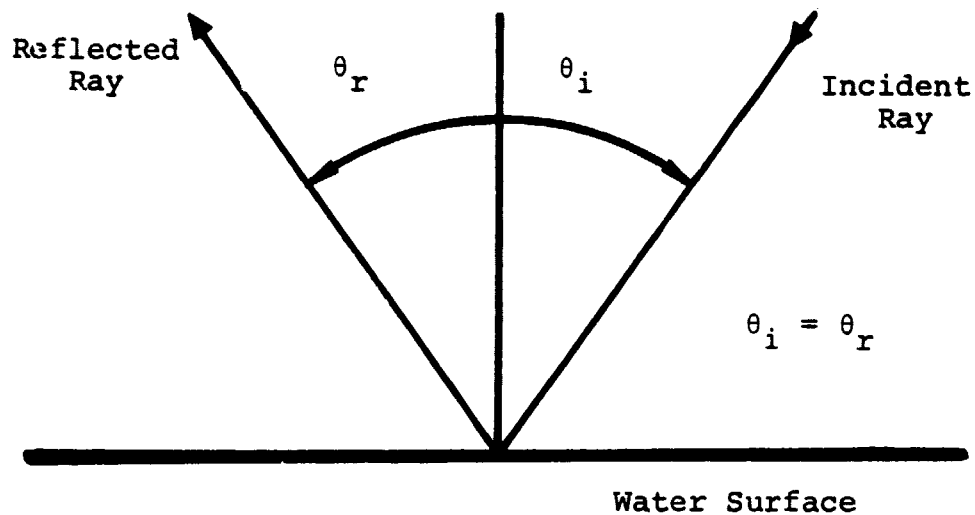


FIGURE 1. SPECULAR REFLECTION FROM A SMOOTH WATER SURFACE.  
THE INCIDENT AND REFLECTED RAYS ARE IN THE  
SAME PLANE.

ORIGINAL PAGE IS  
OF POOR QUALITY

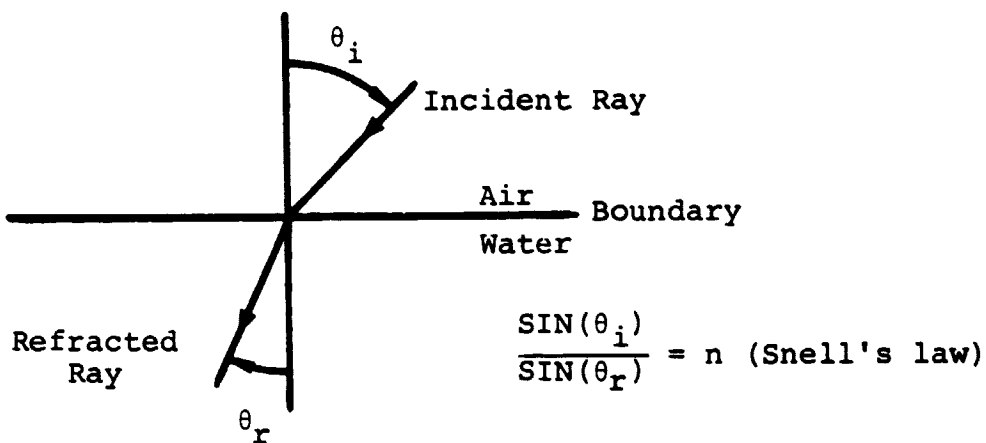


FIGURE 2. REFRACTION OF THE TRANSMITTED BEAM AT THE  
WATER SURFACE AND THE LAW OF REFRACTION  
 $n$  = REFRACTIVE INDEX OF WATER RELATIVE TO AIR.

describes the relationship between the angle of incidence of the incoming beam,  $\theta_i$ , the angle with respect to the normal to the surface of the refracted beam,  $\theta_r$ , and the refractive index of air relative to water. The refracted beam lies in the same plane as the incident beam. The phenomenon of refraction is depicted in Figure 2. The law of refraction requires that for a water surface, downward sky radiation and direct sunlight enter the water within  $48.5^\circ$  of the vertical. Only when the water surface is roughened by wind or another disturbance can direct sunlight or sky radiation penetrate the water surface outside this range of angles. Back-scattered radiation from beneath the water-air interface also experiences refraction on reaching the water surface. When the water surface is calm, upward radiation incident at angles greater than  $48.5^\circ$  with the vertical is totally internally reflected [2]. Thus, downward radiation beneath the water surface at angles with the vertical greater than  $48.5^\circ$  is upward radiation in the water which has been totally internally reflected [3].

Equations 1 and 2 show that the reflectance and transmittance of the water surface are dependent on the refractive index of water. The refractive index is influenced by changes in temperature and by the concentration of various solutes in the water. Figure 3 shows how the reflectance function, equation 1, varies as a function of the angle of incidence for refractive indices of 1.20, 1.33, 1.40, 1.45. This range of refractive indices encompasses the range of natural variability in the refractive index for water; and Figure 3 shows that, over this range, variation in the refractive index is of little importance in determining the surface reflectance. For all of the calculations shown in this report, a refractive index of  $4/3$  is used. Figure 4 shows transmittance,  $T$ , and reflectance,  $\rho_s$ , as a function of angle of incidence of the incoming radiation for a refractive index of 1.33.

Since many applications of remote sensing over water require

ORIGINAL PAGE IS  
OF POOR QUALITY

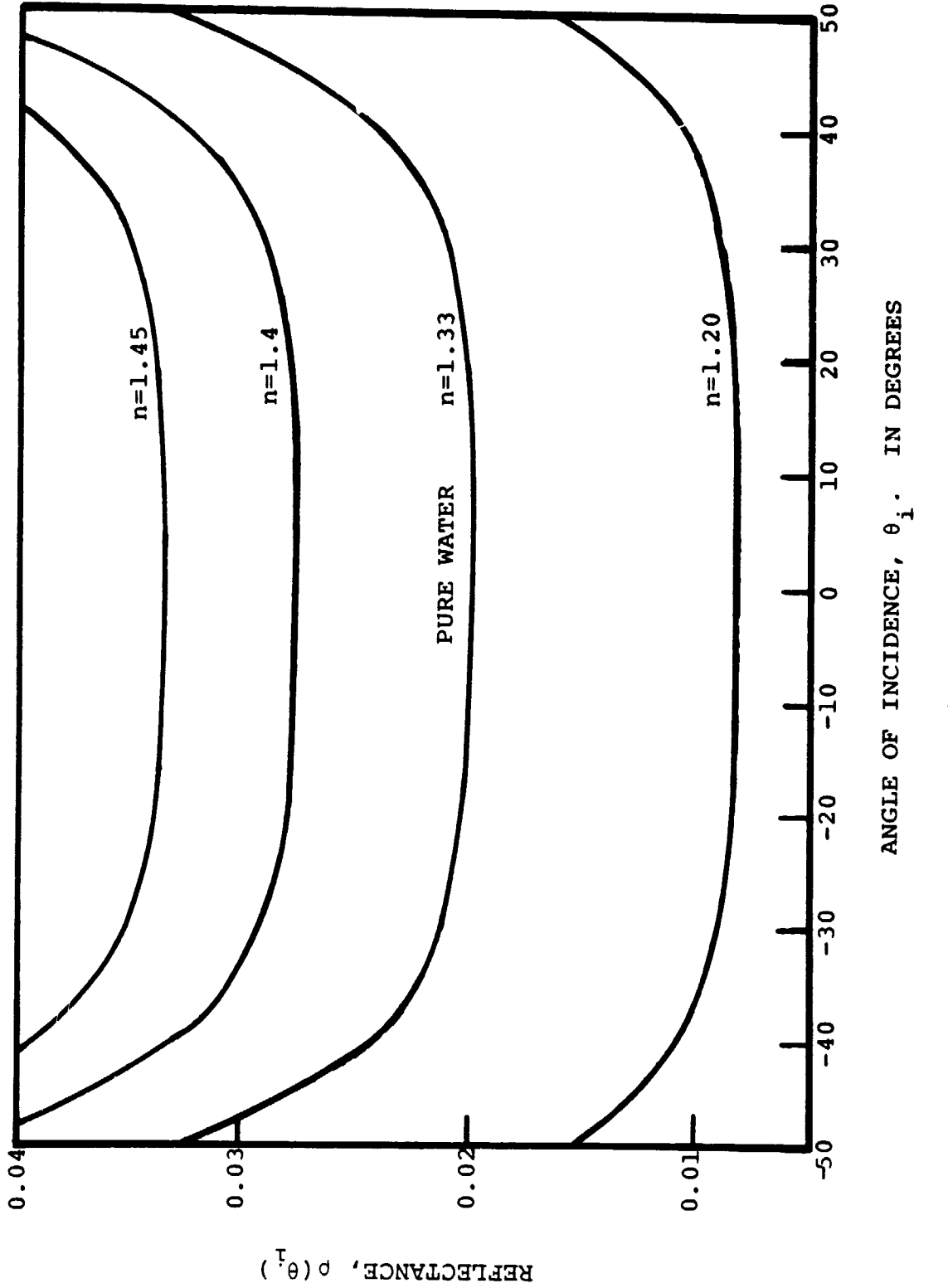


FIGURE 3. FRESNEL REFLECTANCE FOR UNPOLARIZED LIGHT AS A  
FUNCTION OF ANGLE OF INCIDENCE OF INCIDENCE OF INCOMING BEAM.

ORIGINAL PAGE IS  
OF POOR QUALITY

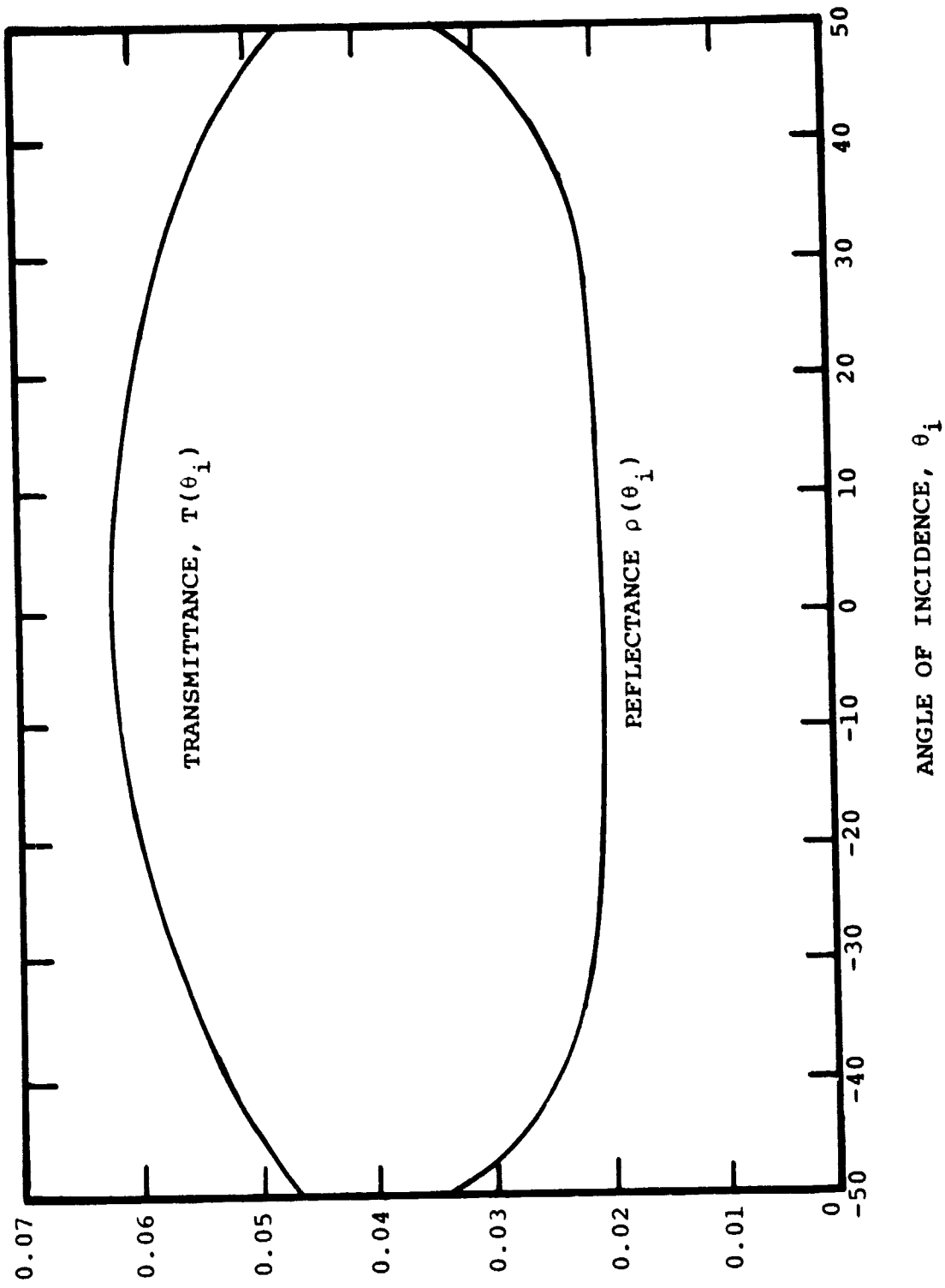


FIGURE 4. FRESNEL REFLECTANCE AND TRANSMITTANCE AS A FUNCTION OF ANGLE OF INCIDENCE OF INCOMING BEAM. REFRACTIVE INDEX = 1.33.

examining the signature from beneath the water surface, Fresnel reflectance is of paramount importance. Figure 4 shows that transmittance is highest when the incident beam is perpendicular to the water surface, while the reflectance is lowest at this angle. Thus, from a consideration of the Fresnel formulas, one would expect the return from beneath the water surface relative to the total, to be greatest when viewing that surface at the nadir. Contributing to this effort is the fact that most scattering phase functions for polydispersions in water have a secondary peak at  $180^\circ$  [2]. Figure 4 shows that while the Fresnel reflectance function is at a minimum at the nadir view angle, this function changes very little out to viewing angles as great as  $40^\circ$ , at which point it begins to rise steeply. Internal reflection at the water surface of upwelling radiation is also at a minimum normal to the water surface. Thus, for remote sensing work where the return from beneath the water surface is of greatest interest, scan angles should be maintained within  $40^\circ$  to  $45^\circ$  of the vertical. Beyond an angle of  $48.5^\circ$  no radiation from beneath the water surface will reach the sensor when the water surface is calm. Scanning in the solar plane is also problematic in this regard since specularly reflected light on the solar side of the scan plane would saturate the sensor. For some purposes, such as viewing the glitter pattern on the water surface, scanning in the solar plane may be desirable.

### 3.2 ABSORPTION AND SCATTERING

Water is a good absorber of electromagnetic radiation. Only in the relatively narrow spectral region from about 400 to 600 nanometers is the transparency of water such that radiation can penetrate more than a few meters in depth below the water surface. Both at wavelengths shorter than 400 nm and longer than 600 nm, absorption increases rapidly and only very small amounts of radiation are scattered back out of the water

into the atmosphere. At the very short wavelengths this radiation is further strongly attenuated in the atmosphere.

Scattering of radiation in water is caused by water molecules, by dissolved salts and by particles in suspension. These effects are usually assumed to be additive [4].

Scattering by water molecules is described by fluctuation theory which predicts scattering of radiation as a result of molecular movements which cause fluctuations in the density of the medium. As in Rayleigh scattering, this type of scattering is proportional to  $\lambda^{-4}$ , where  $\lambda$  is the wavelength of the radiation being scattered. The effect of dissolved salts on the molecular scattering phase function is usually small enough to be neglected.

In general, most scattering in water is accomplished by particles in suspension [4]. Particulate matter in water derives from runoff from land, deposition from the atmosphere, and organic processes within the water. Thus, particles may be quite irregular in shape and particle size distributions are difficult to characterize precisely [2]. Because some sources of particles such as runoff of organic processes may be highly localized in space, size distributions may vary greatly in space and time. Although particle shapes vary considerably from the spherical ideal of scattering theory, it has been shown [5,6] that systems of irregularly shaped particles can be adequately approximated by systems of polydisperse systems of spherical particles. The major observed features of phase functions of particulate suspensions in water are a strong forward scattering peak, a broad minimum around  $100^\circ$ - $130^\circ$  and a small secondary peak in the back scattering direction [4].

### 3.3 OPTICAL PROPERTIES OF A WIND ROUGHENDED WATER SURFACE

Roughness of the water surface caused by wind presents an additional problem in the calculation of the optical properties of the surface. Waves increase the angle of incidence of direct

radiation for high solar elevations. The effect on the Fresnel reflectance, however, is of little consequence since the reflectance does not vary much with solar zenith angle for zenith angles less than  $40^{\circ}$  (see Figure 3). Waves reduce the angle of incidence of direct radiation from a low sun, greatly reducing the reflectance of the water surface. Cox and Munk [7] have shown that wave action becomes a significant factor for solar elevations below  $20^{\circ}$ . At these low sun elevations, reduced reflection, shadowing and multiple reflections greatly reduce the reflected radiance.

The reflection of diffuse radiation by the water surface is little affected by surface roughness [2], although complete agreement on this matter is lacking [8]. Burt [9] found that the albedo of a wind roughened water surface was slightly less than the albedo of a smooth water surface--a decrease from 6.6% to 5.7% for the roughened surface. Cox and Munk [7] measured a small increase in the albedo of a smooth water surface of 5% to 5.5% for a water surface roughened by waves. Kondratyev [8] on the other hand, calculates that where the solar zenith angle is  $0^{\circ}$  the albedo of calm water surface of 2.1% will increase to 13.1%. When the solar zenith angle is  $30^{\circ}$ , the increase will be from 2.2% to 3.8%, and for a solar zenith angle of  $60^{\circ}$  there will be a decrease from 6.2% down to 2.4% for a roughened surface. Plass et al. [10], using a Monte Carlo model of the atmosphere ocean system, demonstrate that the downward flux just below the surface always increases with wind speed, even at high sun elevations. They attribute this result to the fact that more sky radiance near the horizon enters the water when waves are present.

The effect of waves on the radiance of the water surface can be calculated if the probability distribution of surface slopes is known. For an observer looking down on a water surface, the specular angle will vary from place to place over the surface of the water. Since in most remote sensing applications

the light source (Sun) and observer (sensor) are high enough above the surface and the region viewed sufficiently small that variation in the specular angle can be neglected. The radiance of the surface is then directly proportional to the probability of finding a surface element with slope,  $s_0$ , at the specular angle [11]. If  $p$  is this probability, the radiance of the surface,  $L_s$ , at vertical angle  $i$  is given by

$$L_s(i) = L_0(i) \rho_f(i) p \quad (3)$$

where

$L_0(i)$  is radiance incident at the surface at vertical angle  $i$ , and

$\rho_f(i)$  is the Fresnel reflectance at vertical angle  $i$ .

Duntley [12] and Cox and Munk [7,13] have studied the statistical distribution of wave slope as a function of wind speed. Observations of the effect of wind speed on spatially or temporally averaged reflectance of the water surface indicate that it is not significant for view angles less than  $70^\circ$  from vertical. Angles in excess of  $50^\circ$  from the vertical are seldom used in remote sensing systems because of the large optical air mass at these angles.

## COMPONENTS OF REFLECTED AND PATH RADIANCE IN REMOTE SENSING OVER WATER

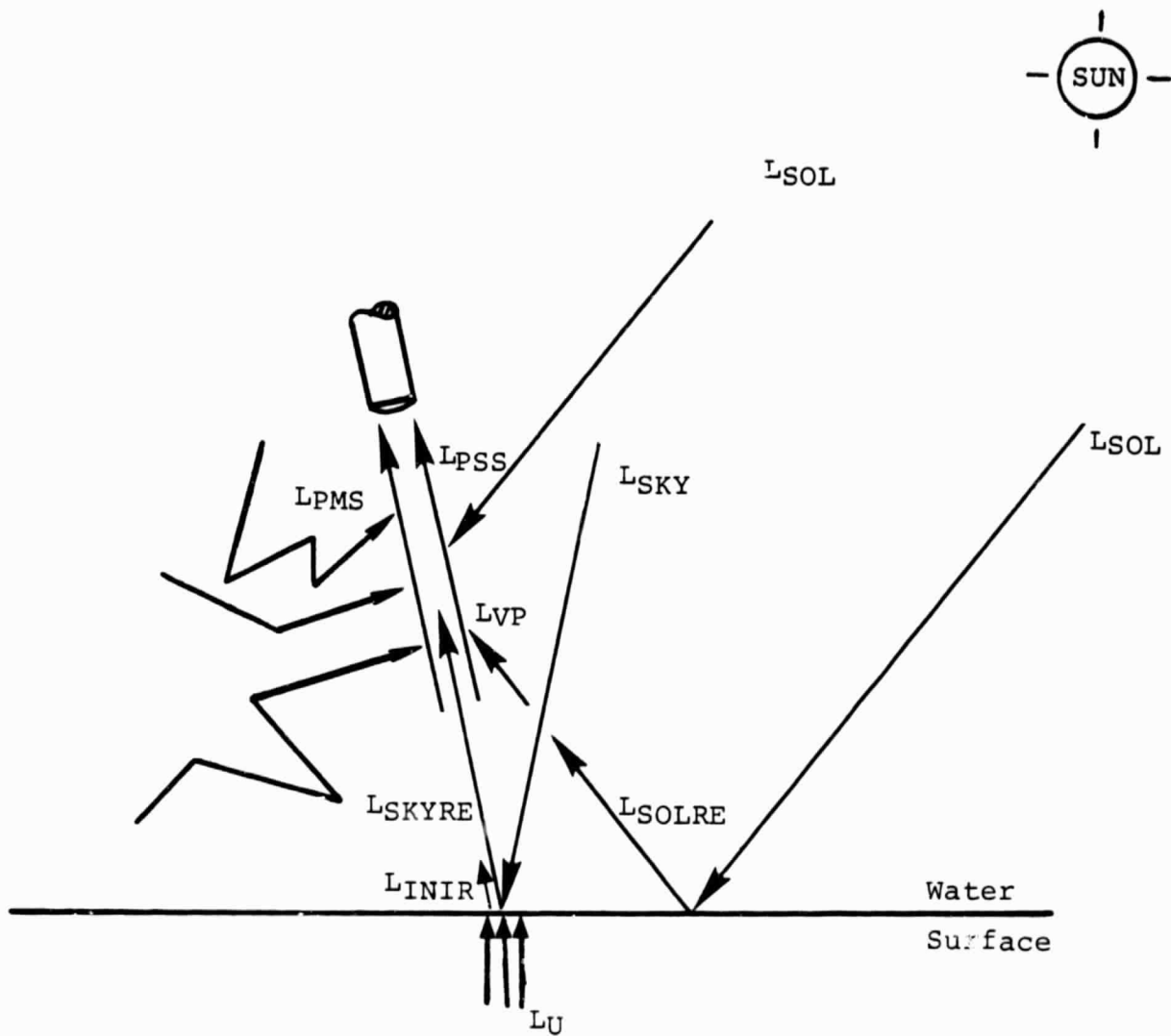
In many applications of oceanographic remote sensing the quantity of greatest interest is the radiance information transmitted from below the water surface to a sensor, sometimes called the intrinsic radiance. To determine this quantity from raw remote sensing data we must not only estimate atmospheric path radiance but also the magnitude of radiance reflected off the water surface and transmitted to the sensor. In this chapter we describe in detail analytical models appropriate for estimating the following quantities: reflected sky radiance, LSKYRE; singly scattered reflected solar path radiance, LVP; singly scattered path radiance, LPSS; and multiply scattered path radiance, LPMS. The first two of these quantities are radiances resulting from specular reflection off the water surface, the latter two are atmospheric path radiances. Each of these radiances augments the radiance detected by a sensor, masking the radiance signal from beneath the water surface, as shown in Figure 5.

### 4.1 REFLECTED SKY RADIANCE, LSKYRE

The geometry for sky radiance reflected into the line of sight of the sensor is depicted in Figure 6, where  $\theta$  represents the nadir view angle of the sensor,  $\phi$  the azimuth of the sensor scanning plane. We assume a plane parallel uniform atmosphere. Sky radiance downwelling in the scan plane and incident at an angle  $\theta$  with the normal to the surface is reflected in the direction of the sensor, and attenuated by the atmosphere as it travels to the sensor. The surface reflectance is given by the Fresnel formula for unpolarized light described in Chapter 3.

We consider in this model only singly scattered sky radiance, generated by scattering of solar beam radiation along the straight

ORIGINAL PAGE IS  
OF POOR QUALITY



$L_{SOL}$  = direct beam radiance;  
 $L_{PMS}$  = multiply scattered path radiance;  
 $L_{PSS}$  = singly scattered path radiance;  
 $L_{SKY}$  = sky radiance;  
 $L_{SKYRE}$  = reflected sky radiance;  
 $L_{SOLRE}$  = reflected solar radiance;  
 $L_U$  = upward scattered radiance beneath water surface;  
 $L_{INIR}$  = radiance scattered from beneath water surface.

FIGURE 5. COMPONENTS OF TOTAL RADIANCE DETECTED BY SENSOR

ORIGINAL PAGE IS  
OF POOR QUALITY

SENSOR

DOWNTWELLING  
SKY RADIANCE

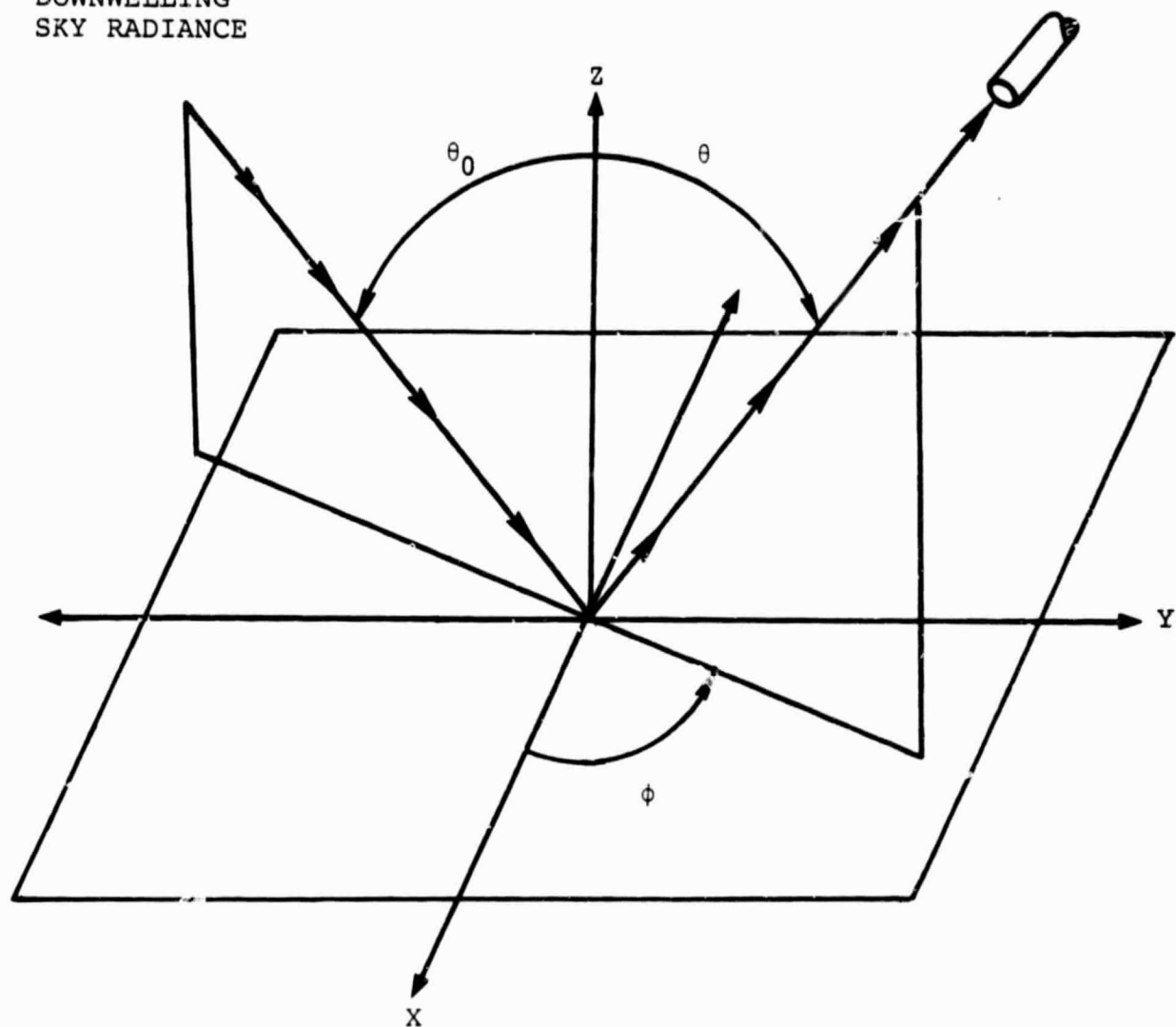


FIGURE 6. GEOMETRY FOR REFLECTED SKY  
RADIANCE COMPUTATION.

line path from the top of the atmosphere to the water surface. In Figure 6, this straight line path has direction  $(-\mu, \phi)$ , where  $\mu = \cos\theta$ . In order to define the angle of scattering we must first define two vectors, one defining the direction of a photon leaving the Sun and the other the direction of the singly scattered sky radiation. If  $(-\mu_0, \phi_0)$  is the direction of the photon leaving the Sun (where  $\mu_0$  is the cosine of the solar zenith angle,  $\theta_0$ , and  $\phi_0$  is the photon azimuth), the vector direction of the photon leaving the Sun is

$$\hat{L}_{SOL} = \begin{bmatrix} \sin(\pi - \theta_0) \cos \phi_0 \\ \sin(\pi - \theta_0) \sin \phi_0 \\ \cos(\pi - \theta_0) \end{bmatrix} = \begin{bmatrix} \sqrt{1 - \mu_0^2} \cos \phi_0 \\ \sqrt{1 - \mu_0^2} \sin \phi_0 \\ -\mu_0 \end{bmatrix} , \quad (4)$$

and

$$\hat{L}_{SKY} = \begin{bmatrix} \sin(\pi - \theta) \cos \phi \\ \sin(\pi - \theta) \sin \phi \\ \cos(\pi - \theta) \end{bmatrix} = \begin{bmatrix} \sqrt{1 - \mu^2} \cos \phi \\ \sqrt{1 - \mu^2} \sin \phi \\ -\mu \end{bmatrix} . \quad (5)$$

The cosine of the scattering angle,  $\chi_{SKY}$ , is given by the dot product  $L_{SOL} \cdot L_{SKY}$ , i.e.

$$\cos \chi_{SKY} = \mu \mu_0 + \sqrt{1 - \mu^2} \sqrt{1 - \mu_0^2} \cos(\phi - \phi_0) . \quad (6)$$

ORIGINAL PAGE IS  
OF POOR QUALITY

The equation for singly-scattered sky radiance,  $L_{SKYSS}$ , is the well-known formula [14]

$$L_{SKYSS} = \frac{\omega_0 \mu_0 E_0 p(x_{SKY})}{4\pi(\mu_0 - \mu)} \left[ e^{-\tau_0/\mu_0} - e^{-\tau_0/\mu} \right] \quad (7)$$

where  $E_0$  = solar irradiance at the top of the atmosphere;  
 $\omega_0$  = atmospheric single scattering albedo;  
 $\tau_0$  = optical thickness of atmosphere;  
 $p(x_{SKY})$  = scattering phase function for scattering angle  $x_{SKY}$ .

When the sky radiance is reflected off the surface of the water it is diminished by the Fresnel reflectance of the water surface,  $\rho_F$ , and further attenuated by the atmosphere on its way to the sensor. Thus, the complete formula for the reflected sky radiance is

$$L_{SKYRE} = \rho_F e^{-(\tau_0 - \tau)/\mu} L_{SKYSS} \quad (8)$$

where  $\mu$  is the cosine of the scan angle,  $\tau$  is the optical depth of the sensor, and  $e^{-(\tau_0 - \tau)/\mu}$  is the transmittance of the atmosphere between the water surface and the sensor. At this point we take note of the fact that in the above formula for the singly scattered reflected sky radiance, the reflectance of the water surface and the transmittance of the atmosphere are opposing effects. Assuming the refractive index of water to be 1.33, the

ORIGINAL PAGE IS  
OF POOR QUALITY

Fresnel reflectance of water at the nadir view angle reaches a minimum of 0.021 and attains a maximum of 1.0 at the grazing angle. Typical values of  $\rho_F$  for angles commonly used in remote sensing range between 2.1 at the nadir to 3.0 at a scan angle of  $46^\circ$ . The transmittance, on the other hand, reaches a maximum at the nadir and becomes increasingly small as the scan angle increases. These effects will be discussed further in the following chapter.

#### 4.2 SINGLY SCATTERED REFLECTED SOLAR RADIANCE, $L_{VP}$ .

The phenomenon of specular reflection produces an image of the radiation source on the surface of the water. We refer to the image of the Sun on the water surface as the virtual Sun. If the scan plane is coincident with the solar plane and the sensor is scanning on the solar side of the scan plane at a view angle equal to the solar zenith angle, the field of view becomes saturated with the radiance of the Sun's image. Radiance from the virtual Sun is also scattered into the line of sight of the sensor. In the terminology of this report, we refer to singly-scattered path radiance from the Sun as virtual Sun path radiance,  $L_{VP}$ .

To find the scattering angle for the computation of singly-scattered virtual Sun path radiance, we note that the zenith angle of a photon leaving the virtual Sun is  $\theta_{SUN}$  and the azimuth angle is  $\phi_0 = \phi_{SUN} + \pi$  (see Figure 7). The vector direction of a photon leaving the virtual Sun is

$$\hat{L}_{VSOL} = \begin{bmatrix} \sin\theta_{SUN} \cos\phi_0 \\ \sin\theta_{SUN} \sin\phi_0 \\ \cos\theta_{SUN} \end{bmatrix} = \begin{bmatrix} \sqrt{1-\mu_0^2} \cos\phi_0 \\ \sqrt{1-\mu_0^2} \sin\phi_0 \\ \mu_0 \end{bmatrix} \quad (9)$$

ORIGINAL PAGE IS  
OF POOR QUALITY

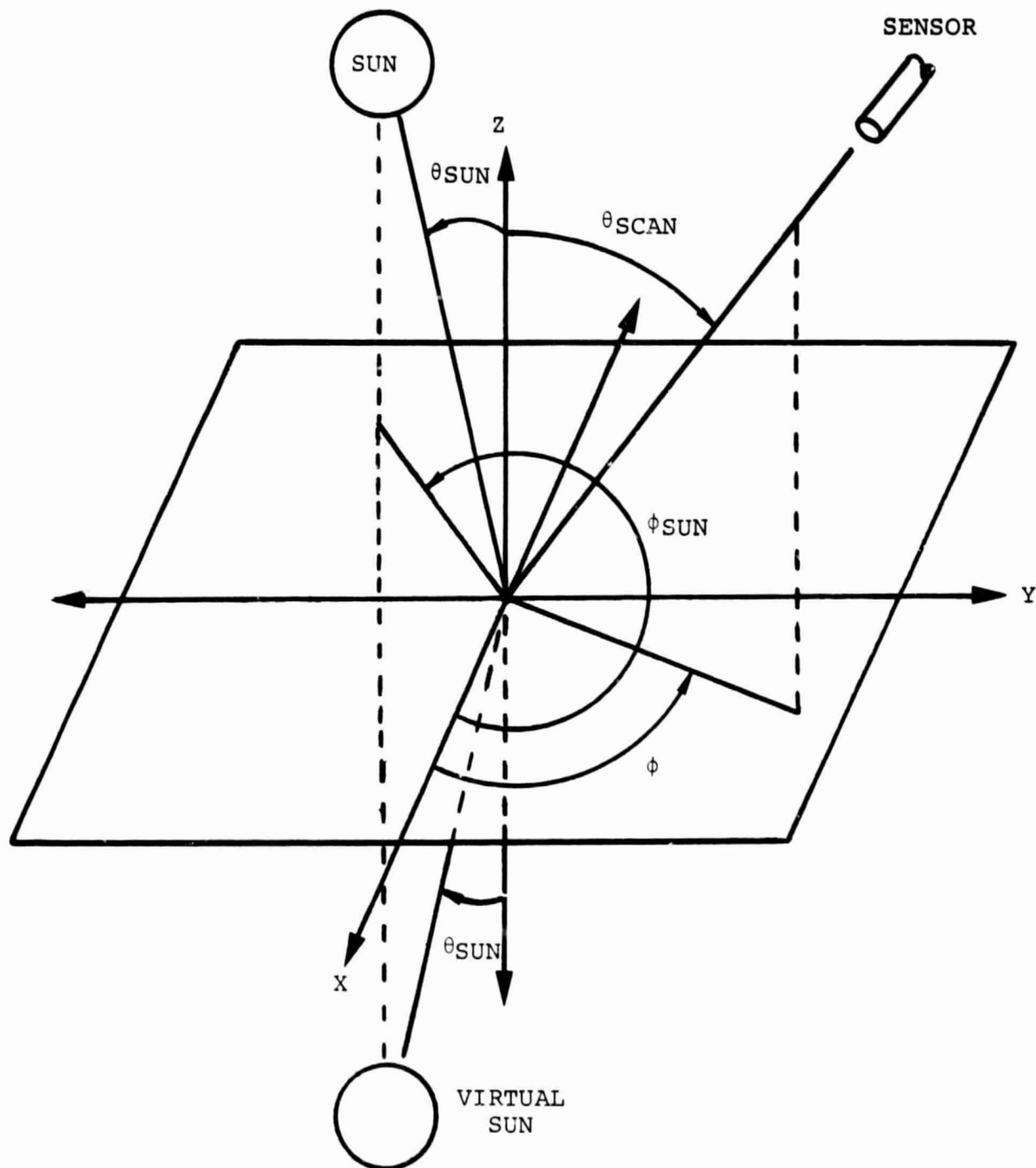


FIGURE 7. GEOMETRY FOR VIRTUAL SUN PATH RADIANCE CALCULATION.

and the vector direction into which photons from the virtual Sun are scattered, creating virtual Sun path radiance is

$$L_{VP} = \begin{bmatrix} \sin\theta\cos\phi \\ \sin\theta\sin\phi \\ \cos\theta \end{bmatrix} = \begin{bmatrix} \sqrt{1-\mu^2} \cos\phi \\ \sqrt{1-\mu^2} \sin\phi \\ \mu \end{bmatrix} . \quad (10)$$

The scattering angle is the dot product,

$$L_{VSOL} \cdot L_{VP} = \mu \mu_0 + \sqrt{1-\mu^2} \sqrt{1-\mu_0^2} \cos(\phi-\phi_0) . \quad (11)$$

As in the case of singly scattered sky radiance, the same types of physical interactions which generate singly-scattered sky radiance from direct solar radiation also scatter radiation from the virtual Sun to generate virtual Sun path radiance. Thus, we may use the same equation for singly-scattered sky radiance, with some modifications, to find the singly-scattered virtual Sun path radiance,  $L_{VP}$ . One difference is in that the computation of  $L_{VP}$  we will now sum the scattered radiation over a path beginning at  $\tau = \tau_0$  (the optical depth of the scene viewed by the sensor) and ending at the optical depth of the sensor,  $\tau$ . If we denote the irradiance of the virtual Sun by  $E_0'$ , we obtain the following formula for singly-scattered path radiance from the virtual Sun:

ORIGINAL PAGE IS  
OF POOR QUALITY

$$L_{VP} = \frac{\omega_0 \mu_0 E_0' p(\cos \chi_{VP})}{4\pi(\mu_0 - \mu)} \left[ e^{-(\tau_0 - \tau)/\mu_0} - e^{-(\tau_0 - \tau)/\mu} \right]. \quad (12)$$

We define  $E_0'$  by noting that the  $E_0'$  is the image of the Sun reflected in the water surface. Hence, the irradiance of the virtual Sun is the irradiance of the true Sun at the top of the atmosphere attenuated by the atmosphere and the reflectance of the water surface, i.e.,

$$E_0' = \rho_F e^{-\tau_0/\mu_0} E_0 \quad (13)$$

where  $\rho_F$  is the Fresnel reflectance and  $e^{-\tau_0/\mu_0}$  is the transmittance of the atmosphere.

#### 4.3 SINGLY SCATTERED PATH RADIANCE, $L_{PSS}$ .

The geometry for singly-scattered path radiance is shown in Figure 8. The formula for singly-scattered path radiance is similar to that for singly-scattered path radiance from the Sun--the same straight line path from  $\tau_0$  to  $\tau$  is used, but  $E_0$  is substituted for  $E_0'$  in the formula. The cosine of the scattering angle for singly-scattered path radiance,  $\cos \chi_{PSS}$  is also the negative of the cosine of the scattering angle used to compute the phase function for  $L_{VP}$ . Thus,  $\cos \chi$  is the dot product,  $\hat{L}_{SOL} \cdot \hat{L}_{VP}$ , vector directions which have already been defined. The formula used to compute singly-scattered solar path radiance is

$$L_{PSS} = \frac{\omega_0 \mu_0 E_0 p(\cos \chi_{PSS})}{4\pi(\mu + \mu_0)} e^{-\tau_0/\mu_0} \left[ e^{(\tau_0 - \tau)/\mu_0} - e^{-(\tau_0 - \tau)/\mu} \right]$$

(14)

ORIGINAL PAGE IS  
OF POOR QUALITY

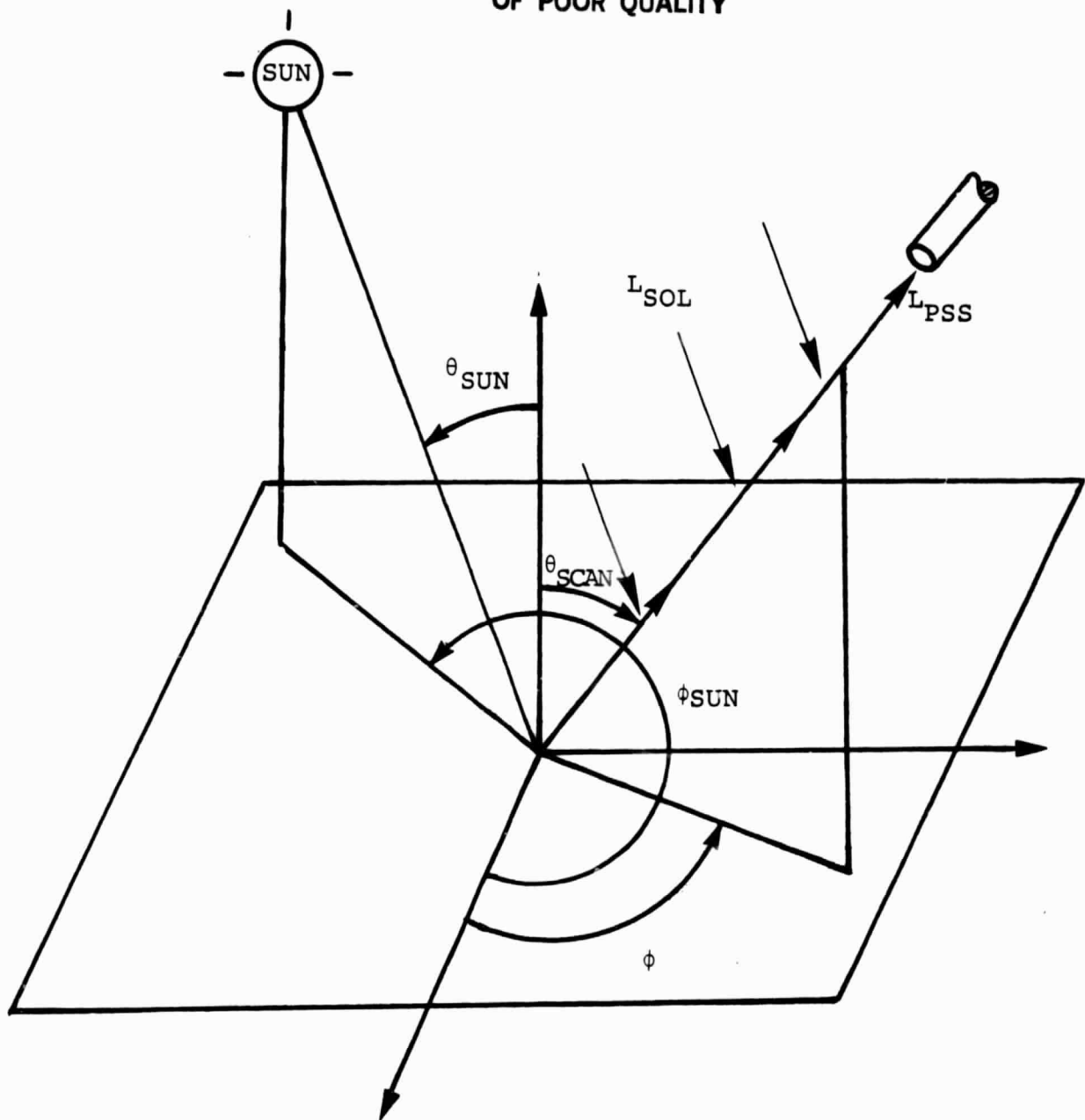


FIGURE 8. GEOMETRY FOR SINGLY SCATTERED PATH RADIANCE,  
 $L_{PSS}$ , CALCULATION.

ORIGINAL PAGE IS  
OF POOR QUALITY

where the variables in the above equation are as previously defined.

4.4 MULTIPLY SCATTERED PATH RADIANCE,  $L_{PMS}$ .

To compute multiply scattered path radiance we use an analytical approximation described in detail in an earlier report [15]. The formula for the computation of  $L_{PMS}$  is

$$L_{PMS} = \frac{E_0}{4\pi [\mu_0 + (1-\eta)\tau_0]}$$

$$\begin{aligned} & \left\{ (1-\eta)\tau_0 [p(\mu, \phi, \mu_0, \pi + \phi_0) + p(\mu, \phi, -\mu_0 \phi_0)] + \mu_0 p(\mu, \phi, -\mu_0 \phi_0) \right. \\ & + \frac{2\mu_0^2 \rho}{1+2(1-\eta)(1-\rho)\tau_0} \left. \right\} \left[ 1 - e^{-(\tau_0 - \tau)/\mu} \right] + \left\{ (1-\eta) p(\mu, \phi, \mu_0, \pi + \phi_0) \right. \\ & + p(\mu, \phi, -\mu_0, \phi_0) \left. \right] - \frac{8(1-\eta)\mu_0^2 \rho}{1+2(1-\eta)(1-\rho)\tau_0} \left[ (\tau_0 + \mu) e^{-(\tau_0 - \tau)/\mu} - (\tau + \mu) \right] \end{aligned} \quad (15)$$

The single-scattering phase functions are given by:

$$p(\mu, \phi, \mu_0, \pi + \phi_0) = p \left[ \mu \mu_0 - \sqrt{(1-\mu^2)(1-\mu_0^2)} \cos(\phi - \phi_0) \right]$$

$$p(\mu, \phi, -\mu_0, \phi_0) = p \left[ -\mu \mu_0 + \sqrt{(1-\mu^2)(1-\mu_0^2)} \cos(\phi - \phi_0) \right].$$

## COMPUTER MODEL AND RESULTS

In this chapter we describe implementation of the formulas discussed in Chapter 4 in the computer program called ATCOR. Many of the details of ATCOR have been presented in a previous report [16], so only a brief description of the entire program will be given here. Our discussion will focus primarily on the subroutine ATMSFR, in which the formulas presented in Chapter 4 have been introduced.

### 5.1 SPECIFICATION OF SOLAR AND SENSOR GEOMETRY

The geometric relationship of the sensor to the environment is shown in Figure 9. The geographic coordinates of the sensor locate the center of a spherical coordinate system used to define angles needed in model calculations. In the diagram the scanner scans along a path from  $P_1$  (the first pixel) to  $P_n$  (the last pixel). The azimuth of the scan plane is measured in the counterclockwise direction from north to the first pixel and is read into the program by the routine ATMSFR. The first pixel is always  $90^\circ$  in a clockwise direction from a vector pointing in the direction of the flight.

The solar zenith and azimuth angles are computed automatically once the latitude, longitude, date, time of day (standard time), and zone number are specified. The extraterrestrial solar irradiance is also computed based on these inputs.

### 5.2 ATMOSPHERIC CORRECTION OPTIONS

Two input parameters set by the user determine which calculations are performed in routine ATMSFR. These parameters are SCATT and OPTION. SCATT may assume the value of either 0 or 1; OPTION can take on the values of 1, 2, or 3. If SCATT is 0, only multiply scattered path radiance is calculated and the value of OPTION can be any integer and will be ignored since only LPMS is then calculated.

ORIGINAL PAGE IS  
OF POOR QUALITY

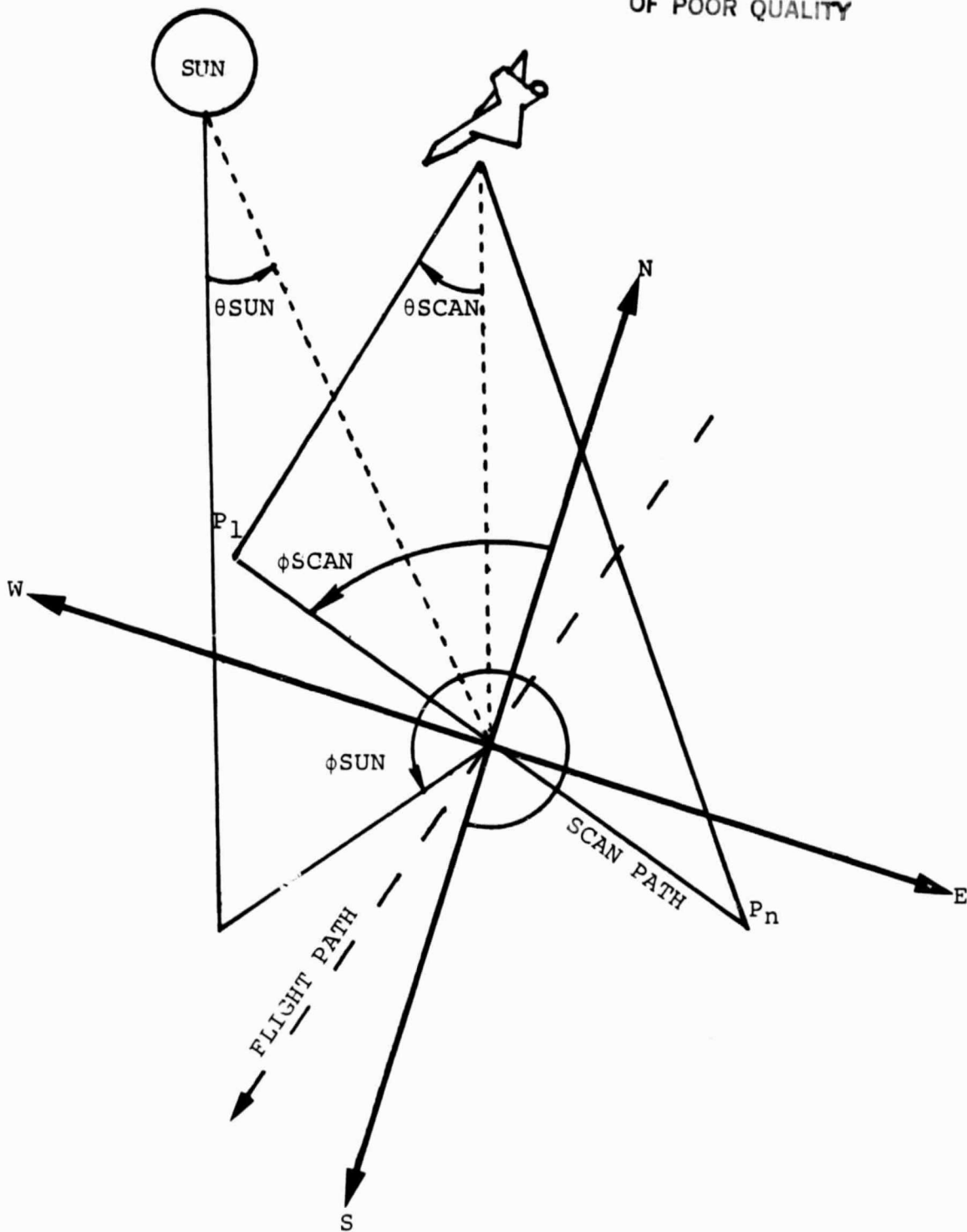


FIGURE 9. SCAN PLANE AND SOLAR GEOMETRY.  $\phi_{SCAN}$  IS MEASURED COUNTERCLOCKWISE FROM NORTH TO PIXEL #1,  $\phi_{SUN}$  IS MEASURED COUNTERCLOCKWISE FROM SOUTH. POSITIVE SCAN ANGLES ARE MEASURED FROM THE FIRST PIXEL TO THE NADIR. NEGATIVE SCAN ANGLES ARE MEASURED FROM THE NADIR TO THE LAST PIXEL.  $P_1$  AND  $P_n$  ARE THE FIRST AND LAST PIXELS, RESPECTIVELY.

If SCATT is 1, single scattering computations are performed and the value of OPTION is used to determine which values to calculate. If OPTION = 1, singly scattered path radiance, LPSS, and reflected sky radiance, LSKYRE, are computed. If OPTION = 2, LPSS and virtual sun path radiance, LVP, are computed. If OPTION = 3, LPSS, LSKYRE and LVP are calculated.

OPTION and SCATT are read into the data file on logical unit 4. The format for this record is (5I5), and the variables read in are:

FSTP    LSTP    PTINC    SCATT    OPTION

where

FSTP = the number of the first pixel to be processed,  
LSTP = the number of the last pixel to be processed,  
PTINC = the pixel increment to use in the processing,  
and SCATT and OPTION are as previously defined.

The output file which is used by ATMSFR is given in Table 1 and the new subroutine ATMSFR2 is given in Table 2.

### 5.3 MODEL INPUT PARAMETERS

In addition to the geometric parameters, we must specify parameters characterizing the medium and the measurement system.

The model makes use of several "altitude" values which must be input by the user. First, one must know the actual altitude (km) of the sensor above the surface. Second, one must know the pressure (millibars) of the atmosphere at the surface, and third, one must know the atmospheric pressure (in millibars) at flight altitude. If only the altitudes are known, one can use the tables relating pressure to altitude as given by the U.S. Standard Atmosphere [17].

**TABLE 1**  
**INPUT FILE ON LOGICAL UNIT 4**  
**FOR USE BY ATMSFR**

**ORIGINAL PAGE IS  
OF POOR QUALITY**

LINE NO.	READ OCCURS IN ROUTINE	INPUT VARIABLES	FORMAT
1	ATMSFR	FSTP,LSTP,PTINC, SCATT,OPTION	(5I5)
2	DATE	MNTH, DAY, YEAR	(3I4)
3	ANGLES	HOUR,MIN,SEC	(2I5,F6.3)
4	ANGLES	NZ	(I5)
5	ANGLES	LATD, LATM, LATS, LONDG, LONGM, LONGS	(2I5,F6.3,2I5, F6.3)
6	ATMSFR	ZSCAN, ZGRND, LSW	(2F8.5,I5)
7	ATMSFR	(WAVE(I), I=1, QNCHAN)	(10F8.5)
8	ATMSFR	(RHO(I), I=1, QNCHAN)	(10F8.5)
9	PHASE	R, IM	(2F8.6)
10 11-14	PHASE	NWT, NANG, (C(I), I=1, NANG)	(2I5/(10F8.6))
15-79	PHASE	(WTAB(I), (PF(I, J), J=1, NANG), I=1, NWT)	(F10.6/(10 F8.4))
80	RAYLEI	PRES0, PRES2	(2F10.4)
81	OZONE	NOZ, NPROF, NO3W1, NO3W2	(4I5)
82	OZONE	WAVC1, WAVC2	(2F8.4)
83-153	OZONE	((ZOZ(IZ), O3INT(IZ, IP), IZ=1, NOZ), IP=1, NPROF)	(F7.0, E11.4)
154	OZONE	(O3MAX(IP), IP=1, NPROF)	(10E13.6)
155-169	OZONE	(WAVO3(I), A(I), I=1, NO3W) (NOTE: NO3W=NO3W1 + NO3W2)	(F7.0,E11.4)

TABLE 1 (Cont.)  
INPUT FILE ON LOGICAL UNIT 4  
FOR USE BY ATMSFR  
(CONTINUED)

ORIGINAL PAGE IS  
 OF POOR QUALITY

LINE NO.	READ OCCURS IN ROUTINE	INPUT VARIABLES	FORMAT
170	OZONE	NOP	(4I5)
171	THICK	NTEX	(I2)
177	THICK	(WAVEX(I), TAUEX(I), I=1, NTEX)	(2F8.4)
178	PARAMS	FSCAT	(10F8.6)
179	AERO	NAER, MPROF, NUZ, MAXG	(5I5)
180	AERO	IPROF	(I5)
181-184	AERO	(WAVAER(I), RIN(I), I=1, NAER)	(10F8.4)
185-230	AERO	((ZUN(IZ), UNIZ(IZ, IP), IZ=1, NUZ), IP=1, MPROF)	(F7.0, E11.4)
231-258	AERO	(X(I), Z(I), I=1, MAXG)	(F7.0, E11.4)
259	ATMSFR	PHID, PHIM, PHIS	(2I3, F6.3)
		\$ENDFILE	

TABLE 2  
PROGRAM LISTING

ATMSFR2

```

1      C*****
2      C*****
3      C*****
4      C*****
5      C*****
6      C*****
7      C THIS IS A MODIFIED VERSION OF THE ROUTINE "ATMSFR" TO BE USED TO
8      C CORRECT FOR ATMOSPHERIC EFFECTS UNIQUE TO LARGE BODIES OF WATER. IT
9      C WILL PERFORM IDENTICALLY AS ITS PREVIOUS VERSIONS WHEN THE VALUE ZERO
10     C ( OR BLANKS ) ARE READ INTO THE INTEGER VARIABLE "SCATT". THUS ANY
11     C PREVIOUS DATA SET MAY BE USED WITH THIS ROUTINE TO PRODUCE THE SAME
12     C MULTIPLY SCATTERED PATH RADIANCE CORRECTIONS.
13     C WHEN SCATT=1, HOWEVER, ATMSFR2 WILL CALCULATE ONLY SINGLY SCATTERED
14     C QUANTITIES. ANOTHER NEW VARIABLE, "OPTION," IS READ IN. WHEN SCATT=0
15     C OPTION HAS NO EFFECT. WHEN SCATT=1, OPTION CHOOSES WHICH RADIANCE
16     C CONTRIBUTIONS TO CORRECT FOR.
17     C IF OPTION=0, ONLY THE PATH RADIANCE PRODUCED BY THE DIRECT SOLAR
18     C RADIATION IS SUBTRACTED FROM THE EXPERIMENTAL RADIANCES. IF OPTION=1,
19     C BOTH THE DIRECT PATH RADIANCE AND THE SKY RADIANCE SPECIALLY RE-
20     C FLECTED FROM THE WATER SURFACE INTO THE SENSOR ARE SUBTRACTED. WHEN
21     C OPTION=2, THE DIRECT PATH RADIANCE AS WELL AS THE PATH RADIANCE PRO-
22     C DUCED BY THE SPECIALLY REFLECTED "VIRTUAL IMAGE" ( I.E. THE "MIRROR
23     C IMAGE" ) OF THE SUN FROM THE WATER IS SUBTRACTED. WHEN OPTION=3, ALL
24     C THREE QUANTITIES ARE SUBTRACTED. ATMSFR2 CALLS ALL AND ONLY THE SAME
25     C ROUTINES AS ITS PREDECESSOR VERSIONS AND IS CALLED IN THE SAME MANNER.
26     C WE DEFINE THE FOLLOWING VARIABLES:
27
28     C LPATH = PATH RADIANCE GENERATED BY THE DIRECT SOLAR RADIATION.
29
30     C LRSKY = REFLECTED SKY RADIANCE OBSERVED AT SENSOR.
31
32     C LVIRP = PATH RADIANCE GENERATED BY THE VIRTUAL IMAGE OF THE SUN OBS-
33     C SERVED AT THE SENSOR.
34
35     C MODIFICATIONS PROGRAMMED BY JIM LIERZER
36     C JAN. 5, 1982
37
38     C INTEGER FUNCTION ATMSFR(L,CONTRL,MCHAN,MSS)
39
40
41
42
43     C VERSION 11LINE/QLINE COMMON BLOCKS VERS. NA3.2 15AUG77 RISH--NASA UNIVAC
44     C VERSION*
45     C     VER.3.0 14APR77 -- 200/24 CHANNEL VERSION ALL PUT TOGETHER
46
47     C     VER.3.0A 6JUN77 -- FINISH MAKING FORTRAN COMPATIBLE. QBREAL
48     C     SWITCH *
49     C     VER.3.0B 7JUN77 -- QBANG, QDANG
50
51     C     VER.3.0C 10JUN77 -- JM'S QANCIL, QIOPAR COMMON BLOCKS ADDED
52
53     C     VER.3.0D 30JUN77 -- QIBSQL; /QANCIL/ IN ALL ROUTINES
54
55     C     VER.3.2 12AUG77 -- MO02. NOT 1.0; QPOLY; QM1.2; Q..999;
56     C     QBSEQL, ETC.
57     C     VER.NA3.2 15AUG77--DIMENSIONS FOR NASA-LEWIS UNIVAC
58
59     C     VER.NA3.3 5JAN82 -- ADDED SINGLE SCATTER, LPATH, LRSKY, LVIRP
60

```

ORIGINAL PAGE IS  
OF POOR QUALITY

TABLE 2 (Cont.)

```

61
62
63 C MAIN COMMON BLOCK FOR USE BY MONITOR, INPUT FSR, MODULES, AND OUTPUT
64 C FSR
65 COMMON /QCOM/, QCVERS(4), QMSAS(6), QMS5, QLINE, QSLINE,
66 QSTEP, QMCHAN, QMSS, QMACH, QFILE,
67 QMNAME, QBPAS1, QBPOLY, QBLSEQL, QBLTID(24), QSPARE(83),
68 QBLSEG, QBLSEG0, QBLSEG1, QBLTSE, QBLREAL, QBLFACT,
69 QITLE(120), QITITL2(120), QLIST(6,20), QSLIST(200),
70 QFACTN(200), QFACT(7A,200), QCM999
71
72 REAL
73 QFACTA, QFACTB, QDANG
74 INTEGER
75 QVERS, QLINE, QMSA, QMSB, QMS, QMA, QMB, QKP, QMS5
76 QFSTL, QLASTL, QSTEPL, QFSTIP, QLASTIP, QSTEPP
77 QSTEP, QMCHAN, QMSS, QMACH, QFILE, QSPARE, QMCHAN
78 QMNAME, QBEND, QBPAS1, QBPOLY, QBLSEG, QBTSE, QBSEGQ,
79 QBLTID, QITLE, QITITL2, QLIST
80 EQUIVALENCE (QMSAS(1), QFSTL, QMSA), (QMSAS(2), QLASTL, QMS5B)
81 EQUIVALENCE (QMSAS(3), QSTEPL, QMS), (QMSAS(4), QFSTIP, QMA)
82 EQUIVALENCE (QMSAS(5), QLASTP, QMB), (QMSAS(6), QSTEPP, QKP)
83 EQUIVALENCE (QCM999, QCM000, QCVERS)
84 C* ANCILLARY DATA COMMON BLOCK
85 COMMON /QACNL/, QDNAME, QAHED(200), QMCIL(180), QAM999
86 INTEGER QDNAME, QAHED, QMCIL
87 LOGICAL QAM999
88 EQUIVALENCE (QAM999, QDNAME)
89
90 C* * * * * C* PARAMETERS* FOR Usc IN FORTRAN PROGRAMS
91 INTEGER QOCHAN, QOCHN2, QOM552, QOIBUF, QOQBUF
92 INTEGER QODILN, QOMX2, QOMX4, QOLD12, QOLCTL
93 INTEGER QUDATA, QURTRY, QUPRNT, QVERR, QUPNCH, QUPRNT, QUSMAP
94 INTEGER QOVRX, QOMREG, QONSEG
95 INTEGER QOCVER(4)
96 C*PARAMETERS -- DECLARATION SIZES FOR DATA ARRAYS
97 DATA QOCHAN/200/
98 DATA QOCHN2/24/
99 DATA QOM552/3264/
100 DATA QOMX2/824/
101 DATA QOMX4/824/
102 DATA QOIBUF/22293/
103 DATA QOQBUF/22293/
104 DATA QUDATA/101/
105 DATA QURTRY/24/
106 DATA QOMREG/24/
107 DATA QONSEG/24/
108 DATA QOLD12/4/
109 DATA QOMX2/2/
110 DATA QOMX4/4/
111 DATA QOLD12/4/
112 DATA QOLD12/4/
113 DATA QOLCTL/4/
114 C*PARAMETERS -- MACHINE DEPENDENT LENGTH ATTRIBUTES, ETC.
115 DATA QUDATA/4/
116 DATA QURTRY/5/
117 DATA QUPRNT/6/
118 DATA QVERR/6/
119 DATA QUPNCH/7/
120 DATA QUPRNT/8/

```

TABLE 2 (Cont..)

```

121 DATA QUMAP /9/
122 C *PARAMETERS -- COMMON BLOCK VERSION TO CHECK THAT ALL MODULES COMPILED
123 C 10 MATCH
124 DATA GOCOVER/ 'VNA3', 'W002', '77/0', '8/15' /
125 C
126 C
127 C
128 C
129 C      INTEGER VERMES(14)
130 C
131 C WHEREVER "10" APPEARS IN THE FOLLOWING DECLARATIONS, IT CAN BE
132 C REPLACED BY THE NUMBER OF CHANNELS. WHEREVER "344" APPEARS, IT
133 C MEANS NUMBER OF POINTS.
134 C
135 REAL L(MCHAN,MSS),MU0,MU0SQ,MU,MU0,MFACT,EFAC(10,344),LPATH(1
136 IO,344)
137 REAL OM(10),ETA(10),A(10),B(10),SIG(10),LAMPP(10),PHIP(10),
138 1 AT(10),BT(10),ATP(10),BTP(10),CIPP(10),CTPP(10),DTPP(10),
139 2 EO(10),E(10),FE(10),FP(10),TAU(10),BHO(10),ALPHA(10),
140 3 G(10),TAUZ(10),MU0(10),LBEM(10),LSURF(10),FSCAT(10),
141 4 RH0(10),LIMR(10),ATPP(10),D(10),WAVE(10),TAS(10)
142 5 TA(10),TR(10),TAU03(10),TAU203(10),TAZ(10),TRZ(10)
143 INTEGER PHID,PHIM,FSIP,LSIP,PTINC,SCATT
144 INTEGER OPTION
145 REAL FRES(344),LRISKY(10,344),LVIRP(10,344)
146 REAL ED(10)
147 REAL AX,REFRAC,AX,SINA,SINB,TANA,TANB,FRESUM,FRESO,
148 1 EFACT,EFACTS,CONST,EXP01,EXP02,COND,COND1,COND2,COND3,
149 2 ARGSKY,ARGVIR,PFVIR,MUFAC1,MUFAC2,ETOTF
150 C
151 C INDEX=REFRACTIVE INDEX OF THE LAKE WATER. WE SET INDEX=1.33. THE
152 C REFRACTIVE INDEX FOR PURE WATER. BUT YOU MAY WISH TO REPLACE
153 C THIS WITH EMPIRICAL VALUES.
154 C FRESO=THE LIMITING CASE OF THE FRESNEL REFLECTANCE AT ZERO ANGLE
155 C OF INCIDENCE THIS WILL VARY WITH "INDEX".
156 C WHEN MU APPROACHES MU0 OR TAU(1) APPROACHES TAUZ(1), THE STAN-
157 C DARD SINGLE SCATTERING RADIANCE FORMULAS TRUNCATE MOST OR ALL
158 C OF THE SIGNIFICANT FIGURES, AND THE EXPONENTIALS IN THEM MUST
159 C BE EXPANDED "COND" CONTAINS THE VALUE TO CHECK AGAINST TO DE-
160 C CIDE WHEN TO USE THE EXPANSIONS. SET COND=10**N(M) WHERE N=
161 C NUMBER OF SIGNIFICANT FIGURES DESIRED. M=MAXIMUM NUMBER OF FI-
162 C GURES HELD BY THE MACHINE. WE TAKE COND=0.01. IN REAL*4 PRE-
163 C CISION AND EXPANSIONS TO FOURTH ORDER TERMS. THIS WILL GUARAN-
164 C TEE RADIANCES TO AT LEAST THREE SIGNIFICANT FIGURES.
165 C
166 DATA INDEX/1.33/,FRESO/0.0200593122/,COND/0.01/
167 INTEGER CONTROL(MSS)
168 DATA PRIOR/0./
169 C*****DATA VERMES/ 'AIMS', 'FR: ', 'TURN', 'ER A', 'TMOS', 'PHER', 'IC M', 'ODEL
170 1', 'RE', 'TSH', 'W VO', 'O 6', '/16', '/77', /
171 DATA OM1/ 9999/
172 DATA EPS/0.001/,PI/3.141592654/
173 C
174 C THESE "DATA" STATEMENTS ARE FOR DEBUGGING ONLY.
175 C
176 C
177 C      DATA WAVE/ .428, .508, .549, .592, .632, .674, .714, .756,
178 C .794/
179 C      DATA LSW/6/
180 C      DATA LSW/2/12.323/

```

TABLE 2 (Cont.)

TABLE 2 (Cont.)

```

241 WRITE(QUPRINT,253)2SC
242 253 FORMAT(' ',19X,'SENSOR ALTITUDE',F10.1,' FEET')
243      Z = ZSCAN-ZGRND
244      C READ SCANNER WAVELENGTHS. ESTIMATED BACKGROUND REFLECTANCES
245      READ (QUDATA,264) (WAVE(1),1-1,QNCHAN)
246      READ (QUDATA,264) (RHO(1),1-1,QNCHAN)
247      FORMAT(10F8.5)
248      CALL PHASE(QUDATA,QUPRNT,QNCHAN,WAVE)
249      CALL RAYLEI(QUDATA,QNCHAN,WAVE,TR,TWZ)
250      CALL OZONE(QUDATA,QUPRNT,QNCHAN,WAVE,Z,TAU03,TAU03)
251      CALL THICK(QUDATA,QUPRNT,QNCHAN,WAVE,TAU)
252      CALL PARAMS(QUDATA,QUPRNT,TR,TAU03,TAU,QNCHAN,ETA,OM,TAS,FSCAT)
253      CALL AERO(QUDATA,QUPRNT,QNCHAN,WAVE,Z,TAU,TR,TAU03,TAZ,TA)
254      MU0 = COS(THETA0)
255      CO2 = 2.*MU0
256      MU0SQ = MU0*MU0
257      CALL SOLAR(WAVE,QNCHAN,NDAY,EO)
258      C CALCULATE ANGULAR QUANTITIES (DEPENDENT ON AZIMUTH ANGLE ONLY)
259      C
260      C READ THE AZIMUTH ANGLE COUNTERCLOCKWISE FROM NORTH TO ( THE FIRST
261      C PIXEL OF THE ) SCAN PLANE.
262      C READ (QUDATA,265) PHID,PHIM,PHIS
263      READ (QUPRNT,270) PHID,PHIM,PHIS
264      WRITE(QUPRNT,'0',19X,'AZIMUTH ANGLE MEASURED COUNTERCLOCKWISE FROM NORTH'
265      ' TO FIRST PIXEL /',28X,'OF SCAN PLANE IS ',13.
266      ' DEGREES, ',13.,' MINUTES, ',13.,' SECONDS. ')
267      2
268      FORMAT(213F6.3)
269      PHI = 1.7453293E-02*PHID + 2.8088821E-04*PHIM + 4.8481362E-06*PHIS
270      FPH = SORT(1.0 - MU0*MU0)*COS(PHI-PHIO)
271      IF (SCATT.EQ.0.OR.OPTION.LT.2) GO TO 301
272      C FIND THE FRESNEL REFLECTANCE OF THE DIRECT SOLAR RADIATION
273      C WHENEVER LVIRP IS DESIRED.
274      C
275      C
276      IF (THETA0)39,43,39
277      39  THEITA=ABS(THETA0)
278      REFRAC=APSN(1/SIN(THETA0)*1./INDEX)
279      AX=THEITA-REFRAC
280      BX=THEITA+REFRAC
281      SINA=SIN(AX)
282      SINB=SIN(BX)
283      TANA=TAN(AX)
284      TANB=TAN(BX)
285      FRESLN=0.5*((SINA*SINA)/(SINB*SINB)+(TANA*TANA)/(TANB*TANB)))
286      GO TO 299
287      43  FRESLN=FRESO
288      299  WRITE(QUPRNT,300)FRESL
289      300  FORMAT(' ',19X,'THE FRESNEL REFLECTANCE FOR THE DIRECT SOLAR '
290      ' RADIATION IS ',F10.5)
291      301  CONTINUE
292      C ECHO A LOT OF DATA TO TELL THE USER THE INPUT DATA WHICH GIVE
293      C HIM THE REST OF THE NUMBERS.
294      C
295      C
296      WRITE(QUPRINT,561)LSM,SCATT,OPTION
297      561  FORMAT(' ',10X,'SWITCH POSITION',3X,11.5X,'SCATTERING MODE',3X,11,
298      ' 5X,'OPTION',3X,11)
299      WRITE(QUPRNT,30)
300      30  FORMAT('0',10X,'ALL RADIANCES ARE IN UNITS OF MILLIWATTS PER CEN'.

```

TABLE 2 (Cont.)

```

1 1 'METER SQUARED'/' 14X, 'PER MICROMETER PER STERADIANT'/
2 1IX, 'ALL IRRADIANCES ARE IN UNITS OF MILLIWATTS PER CENTIMETER'
3 1 ' SQUARED'/'15X, 'PER MICROMETER'/
4 1IX, 'ALL WAVELENGTHS ARE IN MICROMETERS'/
5 IF (SCATT.EQ.0) GO TO 36
6 WRITE(QUPRINT,31)
7 FORMAT(' ',10X,'WE SHALL CALCULATE SINGLY SCATTERED RADIANCES',
8 'ONLY.')
9 IF (OPTION.EQ.0) WRITE(QUPRINT,32)
10 FORMAT(' ',10X,'ONLY THE DIRECT PATH RADIANCE WILL BE CONSIDERED.')
11 IF (OPTION.EQ.1) WRITE(QUPRINT,33)
12 FORMAT(' ',10X,'THE DIRECT PATH RADIANCE AND THE REFLECTED SKY',
13 'RADIANCE WILL BE CONSIDERED.')
14 IF (OPTION.EQ.2) WRITE(QUPRINT,34)
15 FORMAT(' ',10X,'THE DIRECT PATH RADIANCE AND THE VIRTUAL PATH',
16 'RADIANCE WILL BE CONSIDERED.')
17 IF (OPTION.EQ.3) WRITE(QUPRINT,36)
18 FORMAT(' ',10X,'THE DIRECT PATH RADIANCE AND BOTH THE VIRTUAL',
19 'PATH RADIANCE AND THE REFLECTED SKY RADIANCE',
20 'WILL BE CONSIDERED.')
21 GO TO 36
22 WRITE(QUPRINT,37)
23 FORMAT(' ',10X,'WE SHALL CALCULATE MULTIPLY SCATTERED RADIANCES',
24 'ONLY.')
25 CONTINUE
26 WRITE(QUPRINT,275) QDANG,QDANG
27 FORMAT(20X,'MAXIMUM SCAN ANGLE',F9.7,' RADIANS',
28 'ANGULAR RE
29 'SOLUTION OF SCANNER IS ',F9.7,' RADIANS.')
30 WRITE(QUPRINT,276)(1,1=1,ONCHAN)
31 FORMAT('1 CHANNEL',10I10)
32 WRITE(QUPRINT,277)(WAVE(1),1=1,ONCHAN)
33 FORMAT(' - WAVELENGTH',10F10.5)
34 WRITE(QUPRINT,279)(TAU(1),1=1,ONCHAN)
35 FORMAT(' - INTERPOLATED OPTICAL',10F10.5)
36 WRITE(QUPRINT,280)
37 FORMAT(' - THICKNESS')
38 WRITE(QUPRINT,281)(RHO(1),1=1,ONCHAN)
39 FORMAT(' - BACKGROUND ALBEDO',10F10.5)
40 WRITE(QUPRINT,283)(OM(1),1=1,ONCHAN)
41 FORMAT(' - SINGLE SCATTERING',10F10.5)
42 WRITE(QUPRINT,284)
43 FORMAT(' - ALBEDO')
44 WRITE(QUPRINT,285)(FSCAT(1),1=1,ONCHAN)
45 FORMAT(' - SCATTERING PARAMETER',10F10.5)
46 WRITE(QUPRINT,287)
47 FORMAT(' - (FSCAT)')
48 WRITE(QUPRINT,290)(TAUD3(1),1=1,ONCHAN)
49 FORMAT(' - OZONE OPTICAL',7X,10F10.5)
50 WRITE(QUPRINT,292)
51 FORMAT(' - THICKNESS')
52 WRITE(QUPRINT,295)(TR(1),1=1,ONCHAN)
53 FORMAT(' - RAYLEIGH OPTICAL',4X,10F10.5)
54 WRITE(QUPRINT,296)
55 FORMAT(' - THICKNESS')
56 DO 10 I=1,ONCHAN
57 TAUZ(1) = TAUZ03(1) + TRZ(1) + TAZ(1)
58 IF (SCATT.EQ.0) GO TO 500
59 C
60 COMPUTE WAVELENGTH DEPENDENT QUANTITIES NEEDED FOR

```

TABLE 2 (Cont.)

```

3F1 C SINGLE SCATTERING CALCULATIONS
362 C
363 C SIG(1) = TAU(1) - TAUZ(1)
364 C EFACT0 = EXP(SIG(1)/MU0)
365 C CONST = CON*OM(1)*EO(1)
366 C EFACTS = EXP(-TAU(1)/MU0)
367 C ETOTF = (1.-ETA(1))*TAU(1)
368 C E(1) = (MU0*EO(1)/(MU0+ETOTF))*(1.+(2.*RH0(1)*ETOTF)/
369 C (1.+2.*ETOTF))
370 C
371 C IF (E(1)-MU0*EO(1)/E(1)) GO TO 15
372 C COMPUTE DIRECT IRRADIANCE AT SURFACE
373 C ED(1)=MU0*EO(1)*EFACTS
374 C GO TO 15
375 C CONTINUE
376 C
377 C COMPUTE WAVELENGTH DEPENDENT QUANTITIES NEEDED FOR
378 C MULTI SCATTERING CALCULATIONS
379 C
380 C IF (OM(1).GT. OM1) GO TO 20
381 C A(1) = OM(1)*(1.0-ETA(1))
382 C B(1) = 1.0 + A(1) - OM(1)
383 C C = A(1) + B(1)
384 C NU = MU0 / SOR(Y(C*(B(1)-A(1))))
385 C MU0Q(1) = MU0*NU
386 C SIG(1) = TAU(1) - TAUZ(1)
387 C ARG1 = SIG(1)/NU
388 C SH1 = SINH(ARG1)
389 C CH1 = COSH(ARG1)
390 C ARG2 = TAU(1)/NU
391 C SH2 = SINH(ARG2)
392 C CH2 = COSH(ARG2)
393 C ARG3 = C02*ARG2
394 C SH3 = SINH(ARG3)
395 C CH3 = COSH(ARG3)
396 C ARG4 = ARG3*TAUZ(1)/TAU(1)
397 C SH4 = SINH(ARG4)
398 C CH4 = COSH(ARG4)
399 C COMPUTE LAMBDA DOUBLE PRIME
400 C LAMPP(1) = CON*NU0Q(1) * OM(1)*EO(1) / (B(1)*NU*SH2 + MU0*CH2)
401 C COMPUTE PHI PRIME
402 C PHIP(1) = 2.0*RH0(1)*MU050*LAMPP(1)/
403 C (MU0*CH3+NU*(B(1)-A(1))*RH0(1))*SH3
404 C COMPUTE OTHER CONSTANTS
405 C AT(1) = MU*SH1
406 C BT(1) = CH1
407 C ATP(1) = B(1)*NU*SH1 + MU0*CH1
408 C BTP(1) = B(1)*CH1 + MU0*SH1/MU
409 C ATPP(1) = C*NU*SH4 + MU0*CH4
410 C BTPP(1) = 2.0*C*((1.0-OM(1))*NU*SH4 + MU0*CH4)
411 C CTPP(1) = C*NU*SH3 + MU0*CH3
412 C DTPP(1) = 2.0*C*((1.0-OM(1))*NU*SH3 + MU0*CH3)
413 C COMPUTE TOTAL IRRADIANCE AT SURFACE
414 C E(1) = 6.28318531*PHIP(1) * (NU*B(1)*SH3 + MU0*CH3)/
415 C (NU0Q(1)*OM(1)*RH0(1))
416 C FE(1) = MU0*EO(1)/E(1)
417 C COMPUTE DIRECT IRRADIANCE AT SURFACE
418 C ED(1)=MU0*EO(1)*EXP(-TAU(1)/MU0)
419 C GO TO 15
420 C CALCULATE SIMILAR CONSTANTS FOR OMEGA = 1
CONTINUE

```

ORIGINAL PAGE IS  
OF POOR QUALITY

TABLE 2 (Cont.)

```

SF = 1.0-ETA(1)
D(1) = MUO/SF
FP(1) = CONST*SF*EO(1) / (MUO + SF*TAU(1))
CHI = CO2*MUO*RHO(1) / (1.0 + 2.0*SF*(1.0-RHO(1))*TAU(1))
ALPHA(1) = CHI*(4.0 + 1.0/SF)
G(1) = 4.0*CHI
SIG(1) = TAU(1) - TAU(1)
C COMPUTE TOTAL IRRADIANCE AT SURFACE
E(1) = 6.28318531*CHI*FP(1)*(1.0 + 2.0*SF*TAU(1))/(RHO(1)*SF)
FE(1) = MUO*EO(1)/E(1)
C COMPUTE DIRECT IRRADIANCE AT SURFACE
ED(1) = MUO*EO(1)*EXP(-TAU(1)/MUO)
CONTINUE
15
C NOW CALCULATE THOSE QUANTITIES WHICH ARE DEPENDENT ON SCAN ANGLE.
435
436
437 DO 2019 IP=1,IP,1,PT1,INC
438   THETA = QDANG - (IP-1)*QDANG
439   FPHI = FPH
440   IF (THETA .LE. 0.0) FPHI = -FPH
441   MU = COS(THETA)
442   FMU = MU/MUO
443   MUSQ = MU*MU
444   ROOT = SQRT(1.0-MU*MU)
445
446 C THE FOLLOWING EQUATION FOR ARG IS CORRECT. REMEMBER THAT PHI0
447 C IN THIS PROGRAM REPRESENTS THE SOLAR AZIMUTH ANGLE WHILE IN THE
448 C LITERATURE PHI0 USUALLY REPRESENTS THE AZIMUTH ANGLE OF THE DIR-
449 C ECTION OF THE SOLAR RADIATION. THE TWO ANGLES ARE SHIFTED BY 90
450 C DEGREES. CAUSING FPHI TO CHANGE SIGN.
451
452   ARG = FMU + FPHI*ROOT
453   IF (SCATT.EQ.0) GO TO 510
454
455 C BLOCK OF COMPUTATIONS FOR SINGLY SCATTERED RADIANCES.
456 C THESE QUANTITIES DEPEND ON SCAN ANGLE.
457
458   PF2*PF(-ARG,L,TR(1),TAS(1))
459   EXP01=SIG(1)/MU
460   EFACT(1,IP)=EXP(-EXP01)
461   MUFACT=(MU+MU0)/MU0
462   COND1=EXP01*MUFACT
463   IF (ABS(COND1).LT.COND1) GO TO 501
464
465 C CALCULATE SINGLY SCATTERED PATH RADIANCE
466
467   LPATH(1,IP)=(CONST/MUFAC1)*PF2*EFAC1*(EFAC0-EFACT(1,IP))
468   GO TO 502
469
470 C EITHER MU0 AND -MU OR TAU(1) AND TAU(1) ARE TOO CLOSE TO-
471 C GETHER. SO WE MUST EXPAND THE EXPONENTIALS IN THE PATH RADI-
472 C ANCE FORMULA TO FOURTH ORDER TERMS AND CANCEL TERMS.
473
474   LPATH(1,IP)=CONST*PF2*EFAC1*(1.0+COND1/2.)*
475   (1.0+(COND1/3.)*(1.0+(COND1/4.)))
476   IF (OPTION.EQ.0 OR OPTION.EQ.2) GO TO 505
477
478 C NOW CALCULATE THE FRESNEL REFLECTANCE AT THIS SCAN ANGLE.
479 C NEEDED TO FIND THE REFLECTED SKY RADIANCE.
480

```

TABLE 2 (Cont.)

```

481      IF (THETA) 58, 59, 58
482      THETTA=ABS(THEETA)
483      REFRAC=ARSIN(SIN(THETTA)*1./INDEX)
484      AX=THETTA-REFRAC
485      BX=THETTA+REFRAC
486      SINAX=SIN(AX)
487      SINB=SIN(BX)
488      TANA=TAN(AX)
489      TANB=TAN(BX)
490      FRESIP=0.5*((SINA*SINA)/(SINB*SINB)+(TANA*TANA)/(TANB*TANB)))
491      GO TO 310
492      FRESIP=FRSE0
493      CONTINUE
494      C
495      C CALCULATE THE OTHER SCAN ANGLE DEPENDENT QUANTITIES NEEDED
496      C TO FIND THE REFLECTED SKY RADIANCE.
497      C
498      ARGSKY=FMU-FPHI*ROOT
499      PFSKY=PF(ARGSKY, I, TR(I), TAS(I))
500      EXP02=TAU(I)/MU
501      MUFACT2=(MU0-MU)/MU0
502      COND2=EXP02*MFAC2
503      IF (A-(COND2).LT.COND) GO TO 503
504      C
505      C CALCULATE THE REFLECTED SKY RADIANCE
506      C
507      LRSKY(I, IP)=FRES(IP)*(CONST/MUFAC2)*PFSKY*EFAC(I, IP)*
508      1      (EFAC5-EXP(-EXP02))
509      1      GO TO 505
510      C
511      C EITHER MU AND MU0 OR TAU(I) AND TAUZ(I) ARE TOO CLOSE TOGETHER
512      C SO THE FOURTH ORDER EXPANSION OF THE REFLECTED SKY RADIANCE
513      C MUST BE USED.
514      C
515      503      LRSKY(I, IP)=FRES(IP)*CONST*PFSKY*EFAC(I, IP)*EFAC5*EXP02*(1,
516      1      -(COND2/2.)*(1.-(COND2/3.)*(1.-(COND2/4.)))
517      2      ))
518      505      IF (OPTION, LT, 2) GO TO 2019
519      C
520      C CALCULATE THE SCAN ANGLE DEPENDENT QUANTITIES NEEDED TO FIND
521      C THE PATH RADIANCE GENERATED BY THE VIRTUAL SUN.
522      C
523      ARGVIR=FMU-FPHI*ROOT
524      PFVIR=PF(ARGVIR, I, TR(I), TAS(I))
525      MUFACT2=(MU0-MU)/MU0
526      COND3=EXP01*MFAC2
527      IF (ABS(COND3).LT.COND) GO TO 506
528      C
529      C CALCULATE THE PATH RADIANCE GENERATED BY THE VIRTUAL SUN.
530      C
531      LVRP(I, IP)=FRESUN*(CONST/MUFAC2)*PFVIR*EFAC(I, IP)*
532      1      (1./EFAC5)
533      1      GO TO 2019
534      C
535      C EITHER MU AND MU0 OR TAU(I) AND TAUZ(I) ARE TOO CLOSE TOGETHER
536      C SO WE USE THE EXPANSION OF THE VIRTUAL PATH RADIANCE.
537      C
538      506      LVRP(I, IP)=FRESUN*CONST*PFVIR*EFAC5*EFAC(I, IP)*EXP01*(1.+
539      1      (COND3/2.)*(1.+(COND3/3.)*(1.+(COND3/4.))))
540      1      GO TO 2019

```

ORIGINAL PAGE IS  
OF POOR QUALITY

TABLE 2 (Cont.)

```

541      CONTINUE
542      C      CALCULATE THE SCAN ANGLE DEPENDENT QUANTITIES NEEDED TO FIND
543      C      THE MULTIPLY SCATTERED RADIANCE.
544      C
545      C
546      C      IF (OM(1) .GT. OM1) GO TO 52
547      C      DEFINE SINGULARITIES
548      C      SING1 = NUSQ(1) - MU5Q
549      C      SING2 = NUSQ(1) - CO2*CO2*MUSQ
550      C      IF (ABS(SING1) .GT. EPS .AND. ABS(SING2) .GT. EPS) GO TO 55
551      C      WRITE (QUERR,380)
552      C      FORMAT ('--ATMSFR: *****ERROR-- SINGULARITY EXISTS IN EQUATI
      C      ONS*****')
553      C
554      C      ATHT = 57.29578*THETA
555      C      WRITE (QUERR,385) ATHT
556      C      FORMAT (' ATMSFR: SINGULAR AT THETA',F7.4)
557      C      GO TO 2019
558      55      CONTINUE
559      C      PF1 = PF(ARG,1,TR(1), TAS(1))
560      C      PF2 = PF(-ARG,1,TR(1), TAS(1))
561      C      EFAC(1,IP) = EXP(-SIG(1)/MU)
562      C      MFACT = MU * EFAC(1,IP)
563      C
564      C      CALCULATE PATH RADIANCE
565      C      LPATH(1,IP) = LAPP(1) *
      C      1      (A(1)*(AT(1)-BT(1)*MU + MFACT) *PF1
566      C      2      +(ATP(1)-BT(1)*MU -MU*EFAC(1,IP) +B(1)*MFACT)*PF2)/SINA1
567      C      3      +PHIP(1)*
568      C      4      (ATPP(1) +BTPP(1)*MU -CTPP(1)*EFAC(1,IP) -DTPP(1)*MFACT)
569      C      5      /SING2
570      C      GO TO 2019
571      52      CONTINUE
572      C      CALCULATE PHASE FUNCTIONS
573      C      PF1 = PF(ARG,1,TR(1), TAS(1))
574      C      PF2 = PF(-ARG,1,TR(1), TAS(1))
575      C      EFAC(1,IP) = EXP(-SIG(1)/MU)
576      C      CFACT = 1.0 -EFAC(1,IP)
577      C
578      C      CALCULATE PATH RADIANCE
579      C      LPATH(1,IP) = FP(1) *
      C      1      ((SIG(1)-MU*CFACT)*PF1 + (SIG(1) + (D(1)-MU)*CFACT)*PF
580      C      2      2 + (ALPHA(1) + G(1)*MU)*CFACT)
581      C      2019  CONTINUE
582      C      10  CONTINUE
583      C
584      C      ECHO MORE QUANTITIES FOR THE USER'S CONVENIENCE.
585      C
586      C      WRITE (QUPRINT,555)(ETA(1),1=1,QNCHAN)
587      C      555 FORMAT ('- ANISOTROPY PARAMETER',10F10.5)
588      C      WRITE (QUPRINT,291)
589      C      291 FORMAT ('(ETA)', '(ETA)')
590      C      WRITE (QUPRINT,282)(TAUZ(1),1=1,QNCHAN)
591      C      282 FORMAT ('- OPTICAL DEPTH',10F10.5)
592      C      WRITE (QUPRINT,297)(E(1),1=1,QNCHAN)
593      C      297 FORMAT ('- TOTAL IRRADIANCE',4X,10F10.5)
594      C      WRITE (QUPRINT,298)
595      C      298 FORMAT (' ON SURFACE')
596      C      WRITE (QUPRINT,370)(ED(1),1=1,QNCHAN)
597      C      370 FORMAT ('- DIRECT IRRADIANCE',10F10.5)
598      C      WRITE (QUPRINT,371)
599      C      371 FORMAT (' ON SURFACE')
600      C      RETURN

```

ORIGINAL PAGE IS  
OF POOR QUALITY

TABLE 2 (Cont.)

```

C*****C
C  QSTEP=8 -- NEXT LINE TO BE PROCESSED:
C*****C
C  IF WE ARE PRINTING RADIOMETRIC QUANTITIES.  START EACH LINE ON
C  A NEW PAGE.
C*****C
8
C  CONTINUE
601
602  C  QSTEP=8 -- NEXT LINE TO BE PROCESSED:
603
604  C  IF WE ARE PRINTING RADIOMETRIC QUANTITIES.  START EACH LINE ON
605
606  C  A NEW PAGE.
607  IF(LSW.EQ.6) WRITE(QUPRNT,400)
608  FORMAT('1')
609  C  LOOP FOR EACH PIXEL--QNSSS=NUMBER OF PIXELS
610  DO 1009 IP=FSLP,PLSP,PTINC
611  C  TEST "BAD DATA" FLAG FOR THIS PIXEL.  IF NON-ZERO, DON'T PROCESS.
612  IF (CONTRL(IP).NE.0) GO TO 2008
613  DO 3009 IW=1,QNCHAN
614  C  TOTAL RADIANCE (EXPERIMENTAL) = L(IW,IP)
615  LBEAM(IW) = L(IW,IP) - LPATH(IW,IP)
616  IF (SCATT.EQ.0) GO TO 620
617  IF (OPTION.EQ.1 OR OPTION.EQ.3) LBEAM(IW)=LBEAM(IW)-LASKY(IW,IP)
618
619  IF (OPTION.EQ.2) LBEAM(IW)=LBEAM(IW)-LVIRP(IW,IP)
620  CONTINUE
621  IF (L(IW,IP).EQ.0) LBEAM(IW) = 0
622  C  CALCULATE SURFACE RADIANCE
623  LSURF(IW) = LBEAM(IW)/EFFACT(IW,IP)
624  C  CALCULATE INTRINSIC RADIANCE
625  LINTR(IW) = FE(IW)*LSURF(IW)
626  C  CALCULATE SURFACE REFLECTANCE
627  RHOS(IW) = LSURF(IW)/E(IW)
628  GO TO (71,72,73,74,75,76),LSW
629  L(IW,IP) = LPATH(IW,IP)
630  GO TO 60
631  L(IW,IP) = LBEAM(IW)
632  GO TO 60
633  L(IW,IP) = LSURF(IW)
634  GO TO 60
635  L(IW,IP) = LINTR(IW)
636  GO TO 60
637  L(IW,IP) = RHOS(IW)
638  GO TO 60
639  CONTINUE
640  THETA = (QBANG-QDANG*(IP-1)) * 180/PI
641  CONTINUE
642  CONTINUE
643  IF (LSW.NE.6) GO TO 3019
644  C  PRINT RADIOMETRIC QUANTITIES
645  IF(SCATT.EQ.0 OR OPTION.EQ.2) WRITE(QUPRNT,410)
646  C  FORMAT(5X,'LINE NUMBER',16.5X,'PIXEL NUMBER',14.5X,
647  'SCAN ANGLE',F7.3,'DEGREES')
648  C  IF (SCATT.NE.0 AND (OPTION.EQ. OR OPTION.EQ.3)) WRITE(QUPRNT,
649  C  FORMAT(5X,'LINE NUMBER',16.5X,'PIXEL NUMBER',14.5X,
650  'SCAN ANGLE',F7.3,'DEGREES' FRESNEL REFLECTANCE')
651
652  C  WRITE (QUPRNT,420)
653  C  FORMAT('0',14X,'1',9X,'2',9X,'3',9X,'4',9X,'5',9X,'6',
654  '9X,'7',9X,'8',9X,'9',9X,'10')
655  C  WRITE (QUPRNT,425) (L(IW,IP),IW=1,QNCHAN)
656  C  FORMAT('0',140)
657  C  WRITE (QUPRNT,430) (LPATH(IW,IP),IW=1,QNCHAN)
658  C  FORMAT('0',140)
659  C  WRITE (QUPRNT,430) (LPATH(IW,IP),IW=1,QNCHAN)
660  C  FORMAT('0',140)

```

40

TABLE 2 (Cont.)

```

661 IF (SCATT.EQ.0)GO TO 433
662 IF (OPTION.EQ.1.OR.OPTION.EQ.3)WRITE(QUPRINT,431)(LRSKY(IW,IP)
663 ,IW=1,QMCHAN)
664 431 FORMAT(' LRSKY ',10F10.5)
665 432 IF (OPTION.GE.2)WRITE(QUPRINT,432)(LVIRP(IW,IP),IW=1,QMCHAN)
666 433 FORMAT(' LVIRP ',10F10.5)
667 433 WRITE(QUPRINT,434)(EFACT(IW,IP),IW=1,QMCHAN)
668 434 FORMAT(' TRANS ',10F10.5)
669 435 WRITE(QUPRINT,435) LBEAM
670 435 FORMAT(' LBEAM ',10F10.5)
671 440 WRITE(QUPRINT,440) LSURF
672 440 FORMAT(' LSURF ',10F10.5)
673 445 WRITE(QUPRINT,445) LINTR
674 445 FORMAT(' LINTR ',10F10.5)
675 450 WRITE(QUPRINT,450) RHOS
676 450 FORMAT(' RHOS ',10F10.5/'0')
677 C SET QBNONE TRUE TO TELL ANY FOLLOWING MODULES THAT NO OUTPUT
678 C DATA ARE PRESENT.
679 3019 CONTINUE
680 2009 CONTINUE
681 1009 CONTINUE
682 RETURN
683 END
684 END OF FILE

```

ORIGINAL PAGE IS  
OF POOR QUALITY

The user must also define the center wavelengths ( $\mu\text{m}$ ) of the multispectral scanner and the corresponding values of the surface background albedo (values from zero to one). Also, the center wavelengths ( $\mu\text{m}$ ) of the surface radiometers and the corresponding optical thicknesses must be known. It should be noted that the optical thicknesses used should be those measured as closely as possible in time with the multispectral data.

#### 5.4 MODEL CALCULATIONS

In this section we present several examples of the radiances for the various components. Because our main interest is in the radiance components as a function of scan angle and visibility, we will present the results of the calculations in terms of these parameters.

Figure 10 depicts the variation in the singly-scattered reflected sky radiance at the sensor as a function of the nadir scan angle and visibility. In this example the solar zenith angle is  $45^\circ$  and the scan plane is perpendicular to the solar plane. The curves which result are a combination of the variation of the sky radiance, the transmittance from the surface to the sensor, and the Fresnel reflectance of the water surface. For a practical scanner with a maximum scan angle of about  $45^\circ$  the curves indicate that one would not observe the large radiance peaks at the large angles.

In Figure 11 we display the corresponding path radiance as a result of singly-scattered radiation from the reflection of the sun in the water. In this case the radiance peaks do not exist at the large scan angles.

In Figure 12 we illustrate the relative magnitudes of the various radiation components as a function of scan angle for a moderately hazy atmosphere. The virtual sun path radiance is the smallest value and the multiply scattered sky radiance is the largest value.

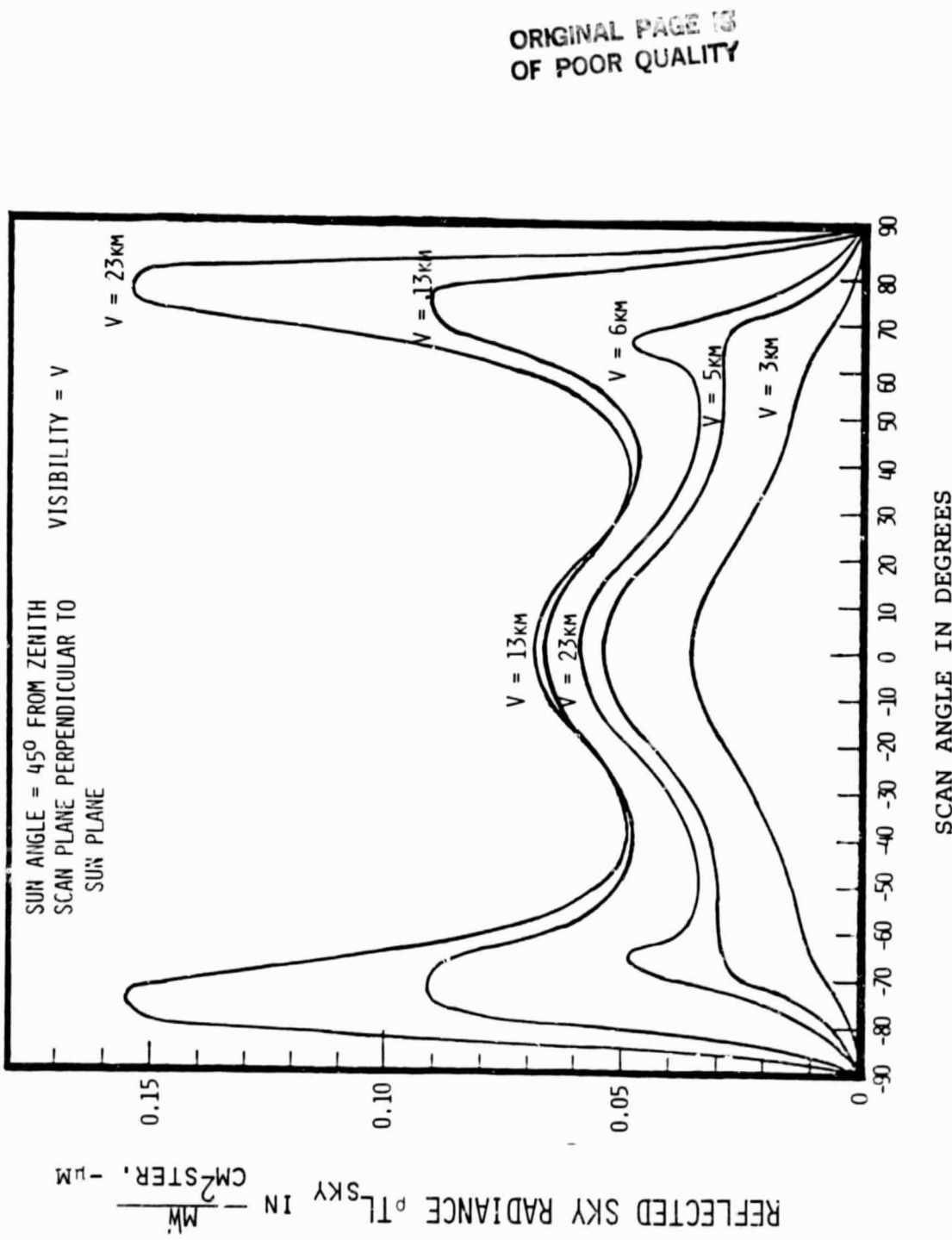


Figure 10. Singly-Scattered Reflected Sky Radiance at Sensor  
for a Wavelength of  $0.55 \mu\text{m}$

ORIGINAL PAGE IS  
OF POOR QUALITY

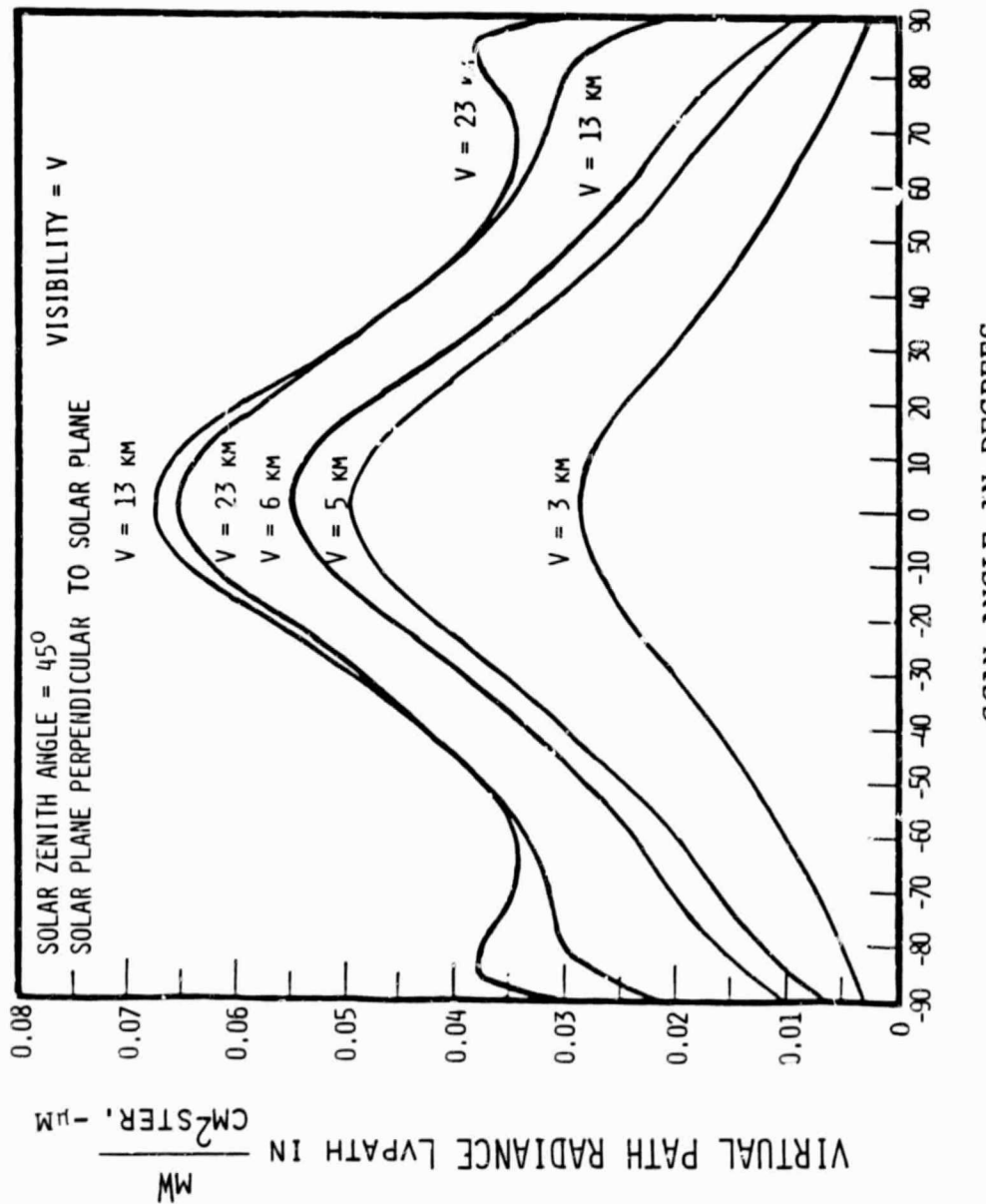
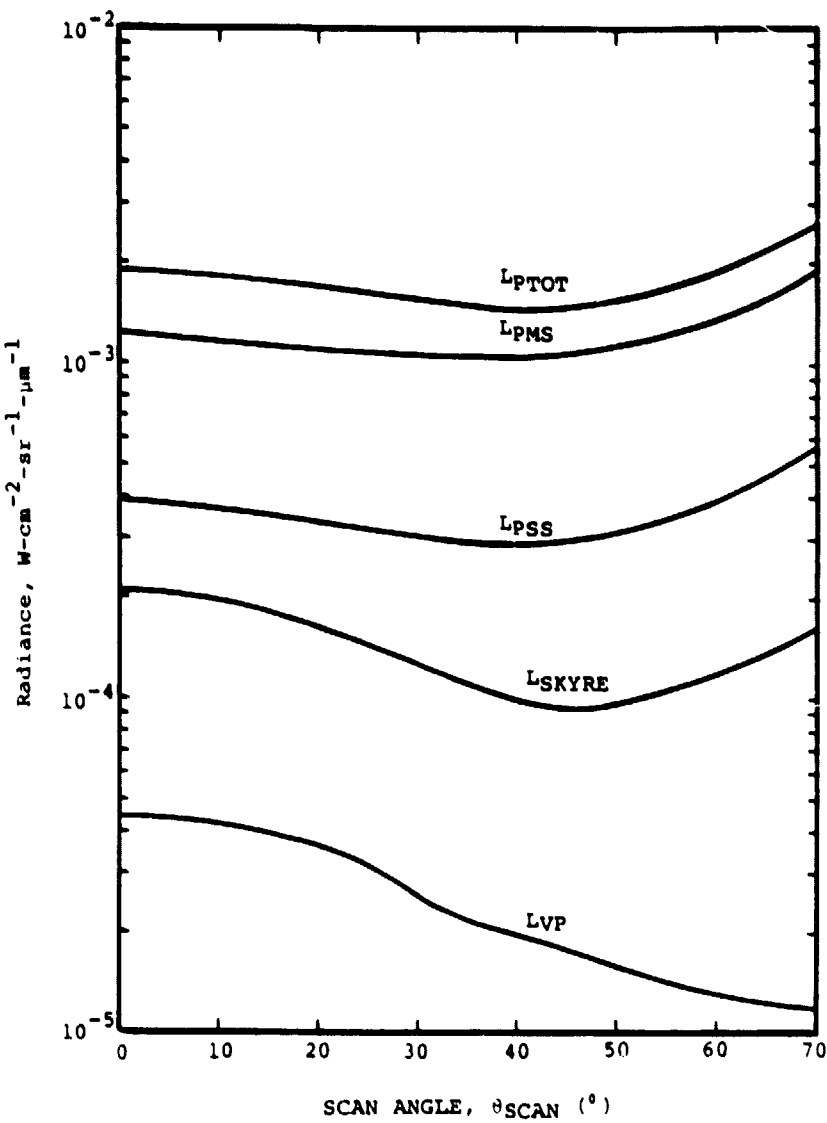


Figure 11. Singly-Scattered Virtual Path Radiance at Sensor  
for a Wavelength of  $0.55\mu\text{M}$

ORIGINAL PAGE IS  
OF POOR QUALITY



- LVP = virtual sun path radiance;
- LSKYRE = reflected sky radiance;
- LPSS = singly scattered path radiance;
- LPMS = multiply scattered path radiance;
- LPTOT = Lvp + LSKYRE + LPSS + LPMS.

Figure 12. SURFACE AND PATH RADIANCE COMPONENTS DETECTED BY SENSOR AT OPTICAL DEPTH OF  $\tau = 0.346$  AS A FUNCTION OF SCAN ANGLE,  $\theta_{\text{SCAN}}$ . SCAN PLANE  $\perp$  SOLAR PLANE,  $\theta_{\text{SUN}} = 30^\circ$ ,  $\lambda = 0.55 \mu\text{m}$ , PHASE FUNCTION = CONTINENTAL REFRACTIVE INDEX 1.5 - 0.01i, VISIBILITY = 10 KM.

In Figure 13 we indicate the variation in the ratio of the singly-scattered sky radiance to the singly-scattered path radiance as a function of the optical depth  $\tau$  of the sensor. As the curves illustrate, the reflected sky radiance component is relatively more important for the larger optical depths.

Figure 14 illustrates the variation in the ratio of the virtual sun path radiance to the singly-scattered path radiance with scan angle for four optical depths.

Figure 15 depicts the large ratio of the multiply-scattered component to the singly-scattered path radiance component as a function of optical depth and scan angle.

Because optical thickness or visibility is of major importance in remote sensing investigations, we want to consider the variation of the radiance components with respect to visibility. This effect is illustrated in Figure 16 for three different atmospheres. We chose the continental aerosol because it more nearly represents the type which would be found over the Great Lakes. The three refractive indices are: 1.5-0.0i which corresponds to a "clean" haze, i.e., one where there is no absorption; 1.5-0.0li which corresponds to a haze with some aerosol absorption; and 1.5-0.li, a complex index of refraction which corresponds to a haze with more absorption. As the curves indicate, an absorbing haze or one which corresponds to considerable air pollution gives rise to a large ratio of reflected sky radiance relative to the singly-scattered path radiance.

The effect of the complex index of refraction is also evident in the ratio of the virtual sun path radiance to the singly-scattered path radiance as indicated in Figure 17.

Finally, we illustrate in Figure 18 the variation of various combinations of ratios in terms of the visibility for a refractive index of 1.5-0.0li.

ORIGINAL PAGE IS  
OF POOR QUALITY

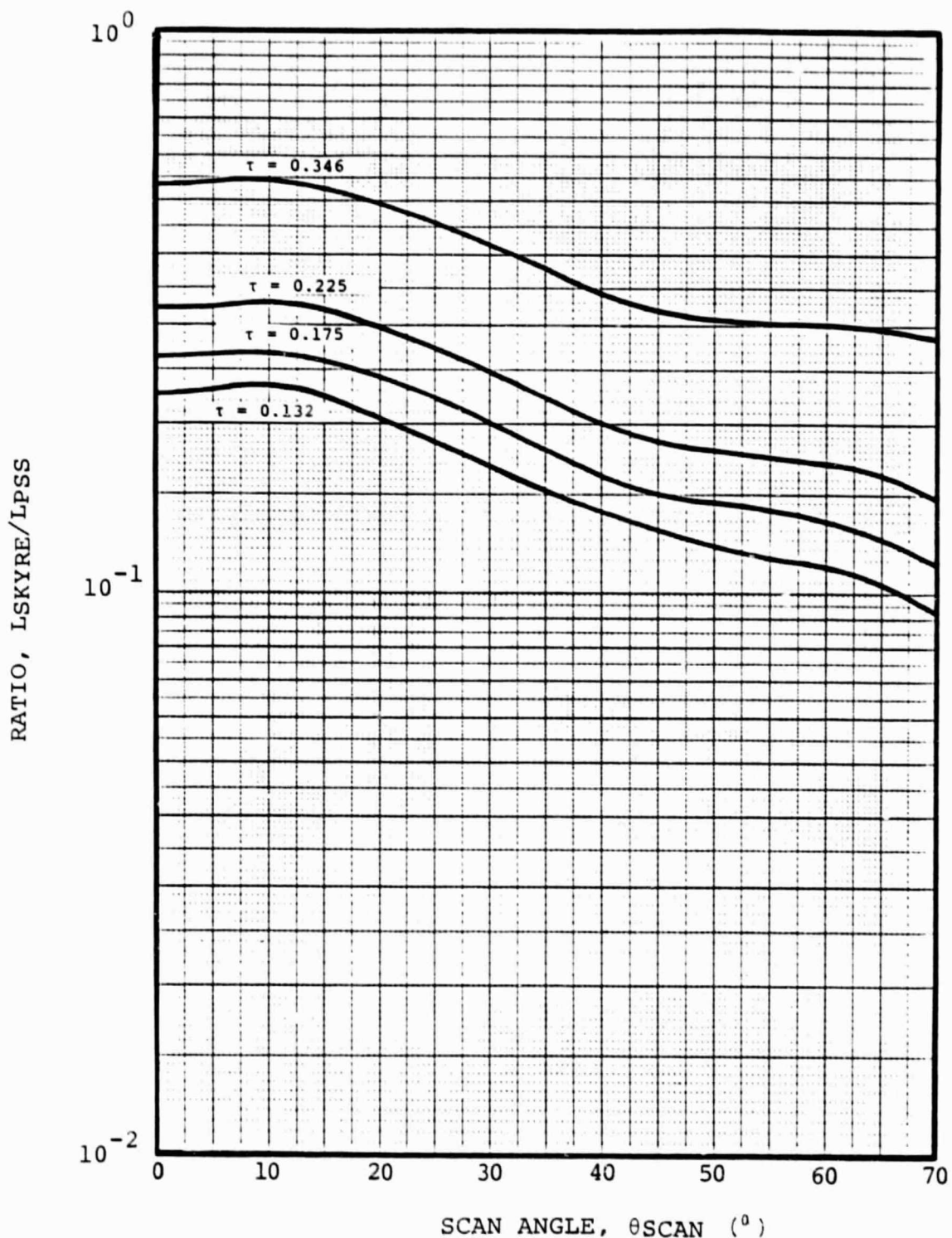


FIGURE 13. RATIO OF REFLECTED SINGLY SCATTERED SKY RADIANCE TO SINGLY SCATTERED PATH RADIANCE AS A FUNCTION OF SCAN ANGLE,  $\theta_{SCAN}$ , FOR OPTICAL DEPTH,  $\tau$ , OF THE SENSOR OF 0.132, 0.175, 0.225 and 0.346. SCAN PLANE  $\perp$  SOLAR PLANE, PHASE FUNCTION = CONTINENTAL REFRACTIVE INDEX 1.5 - 0.01i, VISIBILITY = 10 KM,  $\lambda$  = 0.55  $\mu$ M,  $\theta_{SUN}$  = 30°.

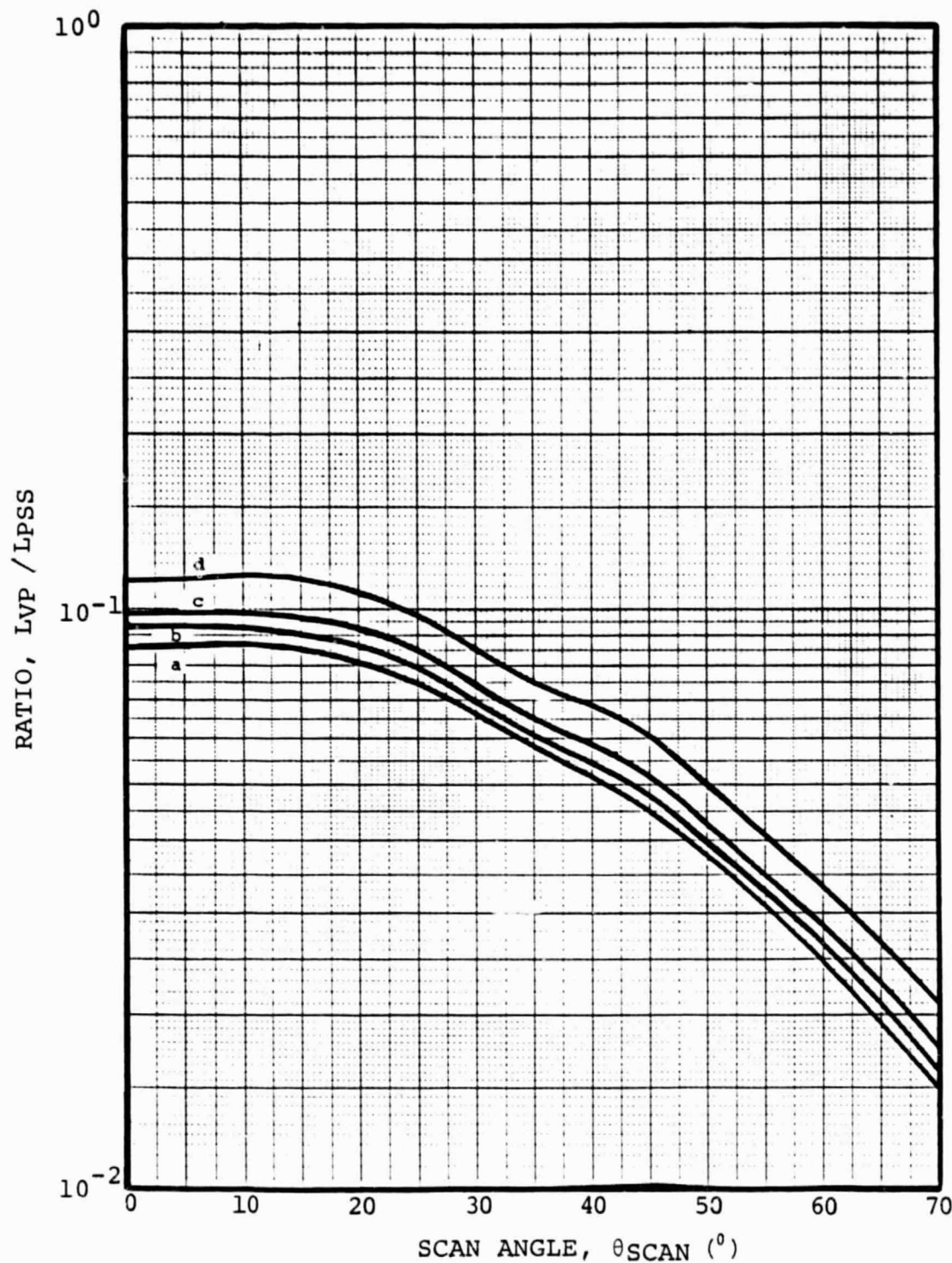


FIGURE 14. RATIO OF SINGLY SCATTERED PATH RADIANCE FROM THE VIRTUAL SUN,  $L_{VP}$ , TO SINGLY SCATTERED PATH RADIANCE,  $L_{PSS}$ , AS A FUNCTION OF SCAN ANGLE,  $\theta_{SCAN}$ , FOR OPTICAL DEPTHS,  $\tau$ , OF THE SENSOR OF A) 0.132, B) 0.175, C) 0.225 AND D) 0.346. SCAN PLANE  $\perp$  SOLAR PLANE, PHASE FUNCTION = CONTINENTAL REFRACTIVE INDEX 1.5 - 0.01i, VISIBILITY = 10 KM,  $\lambda$  = 0.55  $\mu$ M,  $\theta_{SUN}$  = 30 $^{\circ}$ .

ORIGINAL PAGE IS  
OF POOR QUALITY

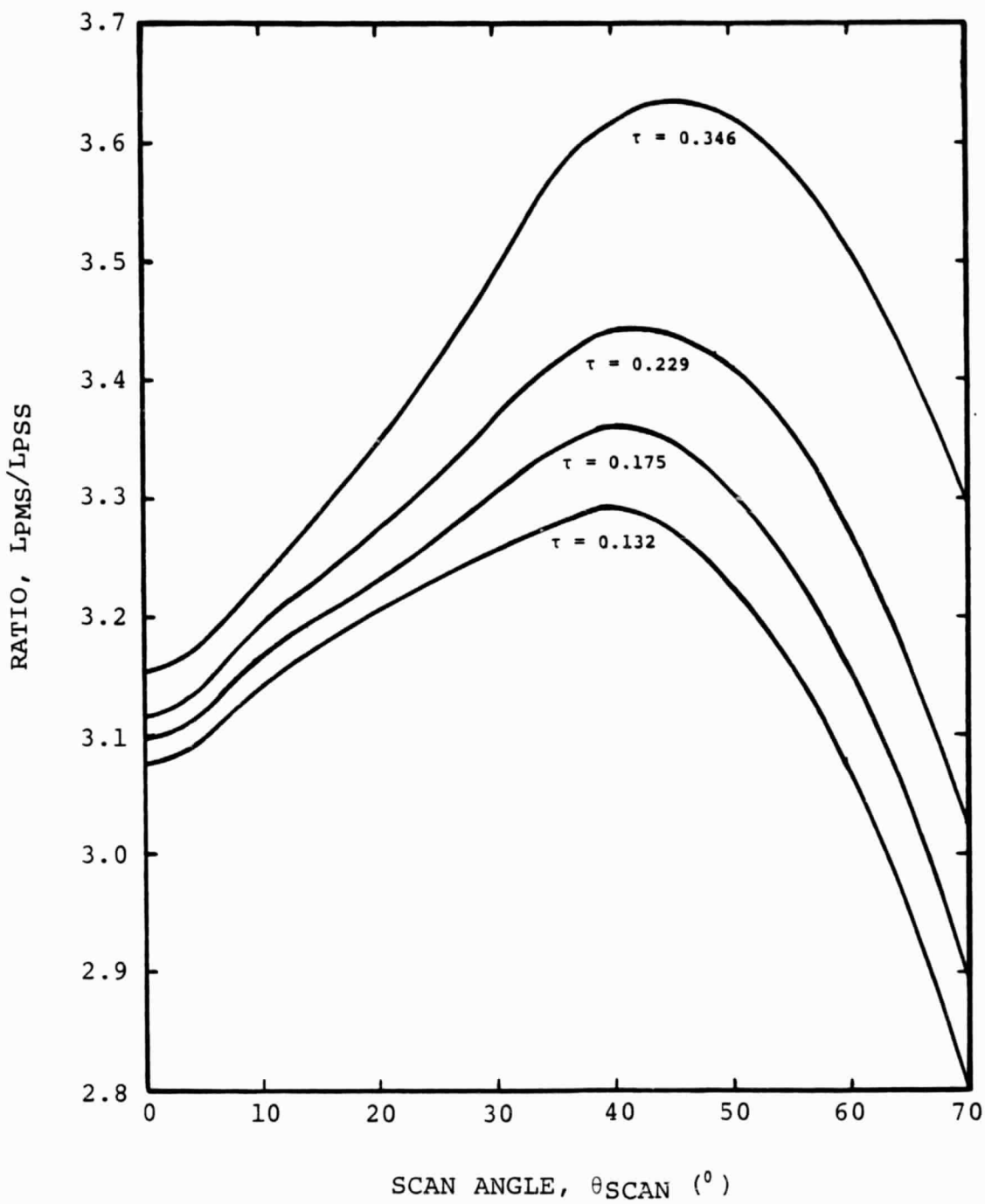


FIGURE 15. RATIO OF MULTIPLY SCATTERED PATH RADIANCE, LPMS, TO SINGLY SCATTERED PATH RADIANCE, LPSS, AS A FUNCTION OF SCAN ANGLE,  $\theta_{SCAN}$ , FOR OPTICAL DEPTHS,  $\tau$ , OF THE SENSOR OF 0.132, 0.175, 0.229, 0.346. SCAN PLANE  $\perp$  SOLAR PLANE, VISIBILITY = 10 KM, PHASE FUNCTION = CONTINENTAL REFRACTIVE INDEX 1.5 - 0.01i,  $\lambda$  = 0.55  $\mu$ M,  $\theta_{SUN}$  =  $30^{\circ}$ .

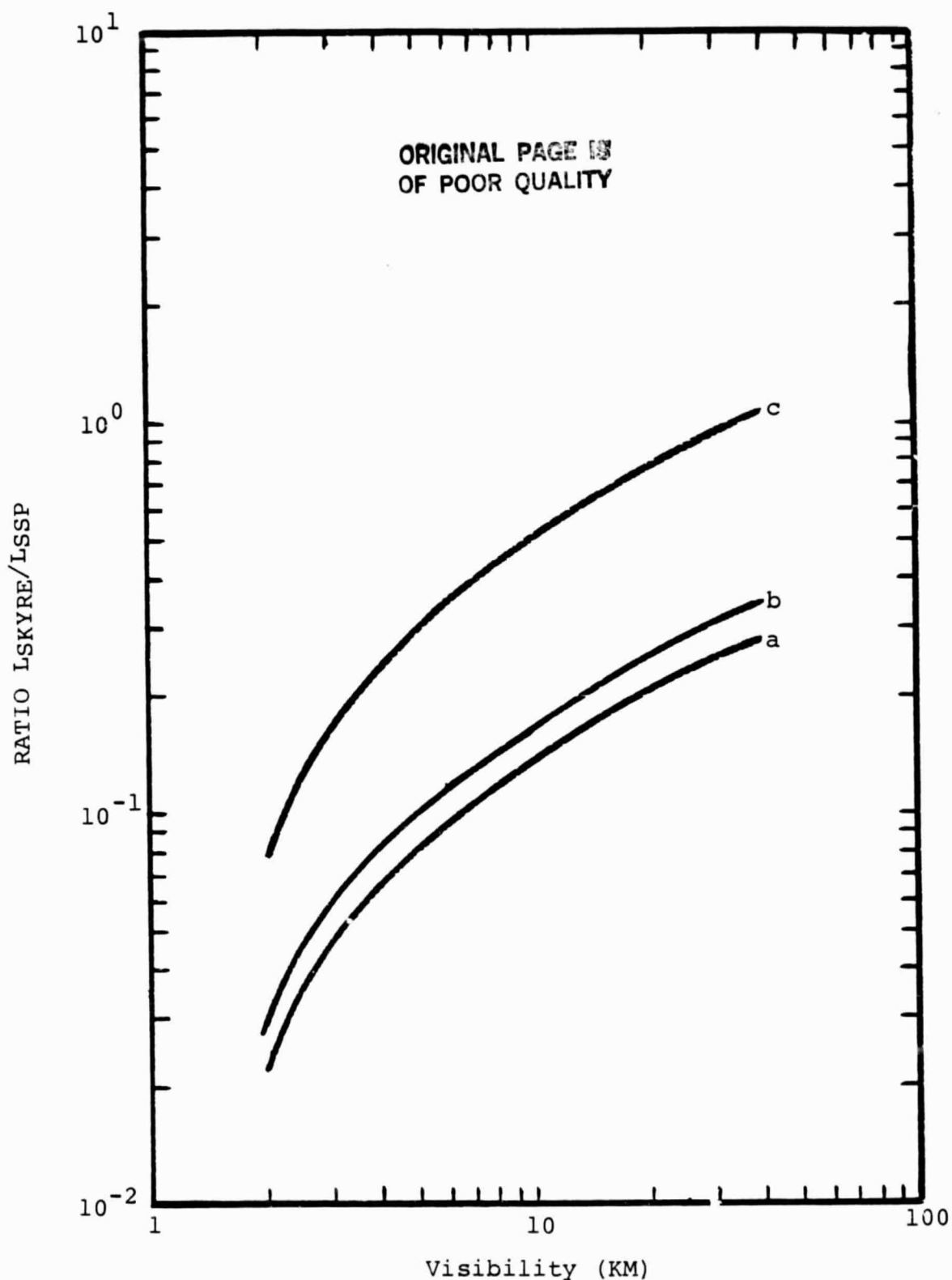


Figure 16. RATIO OF REFLECTED SKY RADIANCE TO SINGLY SCATTERED PATH RADIANCE FOR THREE CONTINENTAL AEROSOL MODELS: a) 1.5 - 0.0i, b) 1.5 - 0.0li, and c) 1.5 - 0.li AS A FUNCTION OF ATMOSPHERIC VISIBILITY. SCAN PLANE  $\perp$  SOLAR PLANE,  $\theta_{SUN} = 30^\circ$ ,  $\lambda = 0.55 \mu M$ .

ORIGINAL PAGE IS  
OF POOR QUALITY

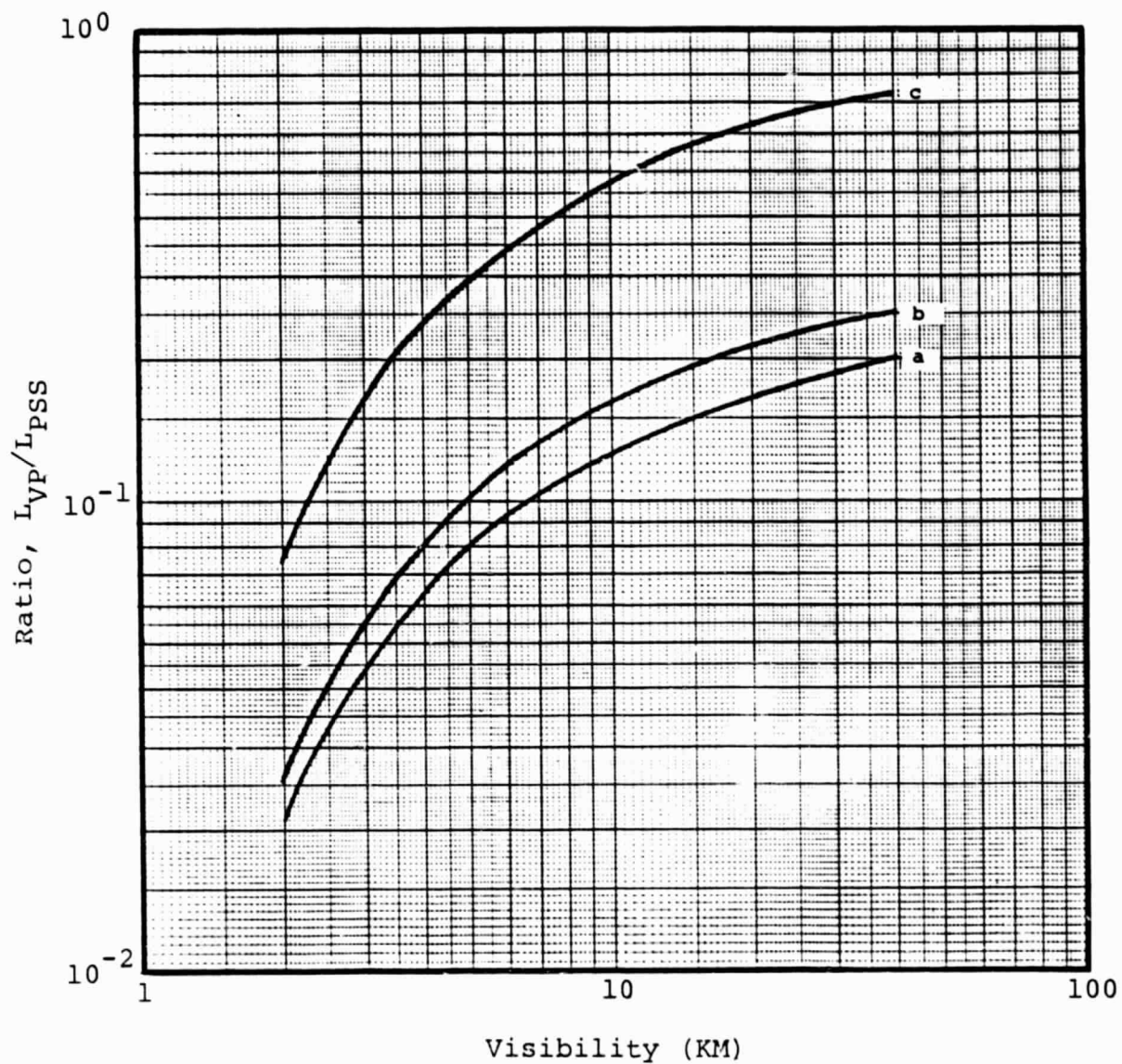
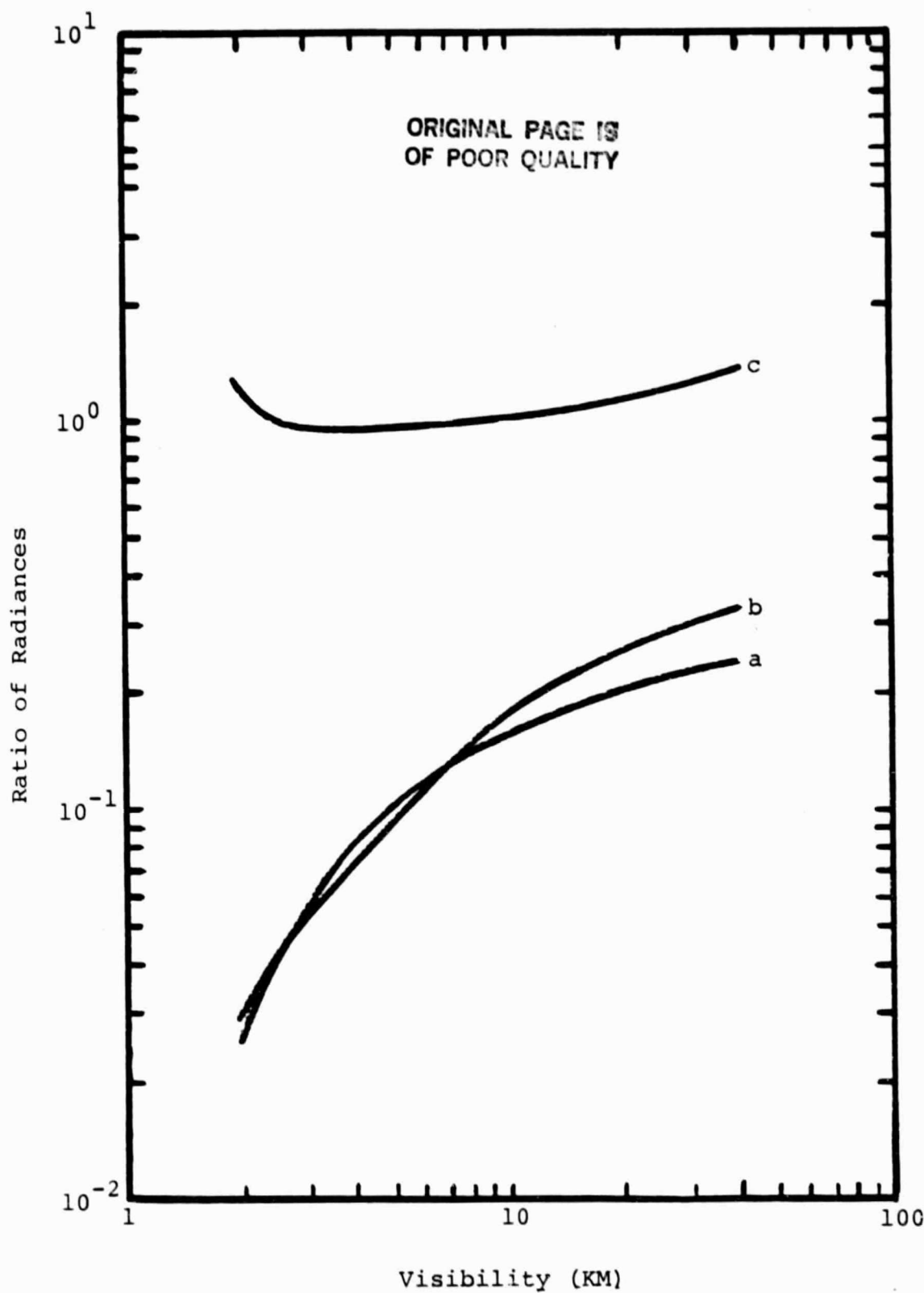


FIGURE 17. RATIO OF SINGLY SCATTERED PATH RADIANCE FROM THE VIRTUAL SUN,  $L_{VP}$ , TO SINGLY SCATTERED PATH RADIANCE,  $L_{PSS}$ , AS A FUNCTION OF ATMOSPHERIC VISIBILITY FOR THREE CONTINENTAL AEROSOL MODELS WITH REFRACTIVE INDICES OF a)  $1.5 - 0.0i$ , b)  $1.5 - 0.01i$ , and c)  $1.5 - 0.1i$ .  $\lambda = 0.55 \mu\text{m}$ ,  $\theta_{\text{SUN}} = 30^\circ$ ,  $\theta_{\text{SCAN}} = 0^\circ$ .



$L_{VP}$  = virtual sun path radiance;

$L_{SS}$  = singly scattered path radiance;

$L_{SKYRE}$  = reflected sky radiance.

FIGURE 18. RATIOS OF (a)  $L_{VP}/L_{SS}$ , (b)  $L_{SKYRE}/L_{SS}$ , (c)  $L_{SKYRE}/L_{VP}$  AS A FUNCTION OF VISIBILITY (KM).  $\lambda = 0.55 \mu\text{m}$ ,  $\theta_{\text{SUN}} = 30^\circ$ ,  $\theta_{\text{SCAN}} = 0^\circ$ , AEROSOL MODEL = CONTINENTAL REFRACTIVE INDEX 1.5 - 0.01i.

## CONCLUSIONS AND RECOMMENDATIONS

The problem of developing an atmospheric correction algorithm for remote sensing is an old and difficult one. The main difficulty lies in not being able to have available sufficient data which can be used to specify the values of the relevant atmospheric parameters. The problem is all the more difficult in the case of the remote sensing of water bodies because of the low signal-to-noise ratio involved. In this investigation we have extended an existing computer algorithm so as to include additional radiation components. The original algorithm included the path radiance which arises from the singly-scattered solar radiation in the atmosphere. We have now included the radiance which arises from the sky radiation which is reflected by the water surface and is then attenuated as it propagates from the surface to the sensor. In addition, we have included the path radiance component which arises from the single scattering of radiation as a result of a virtual sun, i.e., of the sun's reflection in the water. It should be realized that this component is always present regardless of the scan plane, i.e., it does not only occur when the scanner is looking at the specular angle. In addition to these components, we have also included a multiple-scattering approximation. It should be realized, however, that the multiple scattering applies only to an atmosphere with the sun as a source. Another multiple scattering calculation should be performed to include the effect due to the virtual sun.

The general result of all these calculations indicates that the various components are all about equal in magnitude but that there is considerable variation with respect to scan angle and visibility. Also, it appears that the multiply-scattered component is of major significance.

It must be pointed out that the objective of this investigation is to provide an algorithm for the correction of remotely sensed data for atmospheric effects so that one can extract from the multi-spectral data the radiance which is characteristic of the water itself. In our investigation we have dealt with the water surface as a flat, specular reflector, which in general is not true. A wind-roughened surface will be characterized by a complex wave structure which leads to a more complicated representation of the reflected and virtual sun radiances than presented in this report. A further investigation should be conducted to model the water surface in terms of wind speed and a stochastic representation of the reflecting facets of the water surface. If this is done, then a more realistic model could be developed which should provide better values for the sky-reflected and the virtual sun path radiances. It may even be possible to establish a method for the determination of wind speed by observing the average radiance as a function of the instantaneous field of view.

A further recommendation is to improve the accuracy of the algorithm by including a more detailed calculation of the multiply-scattered path radiance, both for the direct sun as a source and for the virtual sun as a source.

## REFERENCES

1. Austin, R. W., 1974: The Remote Sensing of Spectral Radiance from Below the Ocean Surface. In Optical Aspects of Oceanography, N. G. Jerlov & E. S. Nielsen (eds.) Academic Press, New York, pp 317-344.
2. Jerlov, N. G., 1976: Marine Optics. Elsevier, New York, p. 229.
3. Plass, G. N. and Kattawar, G. W., 1969: Radiative Transfer in the Atmosphere-Ocean System. Applied Optics, 8, pp 455-466.
4. Kullenberg, G., 1974: Observed and Computed Scattering Functions. In Optical Aspects of Oceanography, Academic Press, N. G. Jerlov and E. S. Nielsen (eds.), New York, pp 25-49.
5. Beardsley, G. F., Jr., 1968: Mueller Scattering Matrix of Sea Water, J. Opt. Soc. Am., 58, pp. 52-57.
6. Holland, A. C. and Gagne, G., 1970: The Scattering of Polarized Light by Polydisperse Systems of Irregular Particles, Applied Optics, 9, pp 1113-1121.
7. Cox. C. and Munk, W., 1956: Slopes of the Sea Surface Deduced from Photographs of Sun Glitter, Bull Scripps Inst. Oceangr. University of California, 6, pp 401-488.
8. Kondratyer, K. Y., 1969: Radiation in the Atmosphere, International Geophysics Series, Academic Press, New York 912 pages.
9. Burt, W. V., 1954a: Albedo Over Wind-Roughened Water, J. Meteorol. II, pp. 283-290.
10. Plass, G. N., Kattawar, G. W. and Guinn, J. A., Jr., 1975: Radiative Transfer in the Earth's Atmosphere and Ocean: Influence of Waves, Applied Optics, 14, pp. 1924-1936.
11. Cox. C. S., 1974: Refraction and Reflection at the Light Surface. In Optical Aspects of Oceanography, Academic Press, N. G. Jerlov and E. S. Nielsen (eds.), New York, pp. 51-76.
12. Duntley, S. Q., 1950: The Visibility of Submerged Objects: Part I. Optical Effects of Water Waves. Ref. Visibility Lab., Mass. Institute of Technology, Dec. 15, 1950; U.S. Off. Naval Research Rep. No. N5 ori-07831.
13. Cox. C. S., and Munk, W., 1954: Statistics of the Sea Surface Derived from Sun Glitter, Journal of Marine Research, 13, pp. 198-227.

REFERENCES (Continued)

14. Turner, R. E., 1974: Radiative Transfer in Real Atmospheres, NASA CR-ERIM 190100-24-T, Final Report.
15. Turner, R. E., 1976: Investigation of Earth's Albedo Using Skylab Data, NASA CR-ERIM 102200-20-F, Final Report.
16. Turner, R. E., 1977: Atmospheric Transformation of Multi-spectral Remote Sensor Data, NASA CR-135338.
17. U.S. Standard Atmosphere, 1976: NOAA-S/T 76-1562, U.S. Government Printing Office.